Journal of Structural Geology 145 (2021) 104306

Contents lists available at ScienceDirect

Journal of Structural Geology

journal homepage: http://www.elsevier.com/locate/jsg

The role of structural reactivation for gold mineralization in northeastern Hunan Province, South China

Yueqiang Zhou [a,b,c], Deru Xu [d,*], Guojun Dong [c], Guoxiang Chi [e], Teng Deng [d], Jianxin Cai [f], Juntao Ning [c], Zhilin Wang [g]

[a] Key Laboratory of Mineral and Metallogeny, Guangzhou Institute of Geochemistry, Chinese Academy of Sciences, Guangzhou, 510640, China
[b] University of Chinese Academy of Sciences, Beijing, 100049, China
[c] Team 402, Hunan Geology and Mineral Resources Exploration and Development Bureau, Changsha, 410014, China
[d] State Key Laboratory of Nuclear Resources and Environment, East China University of Technology, Nanchang, 330013, China
[e] Department of Geology, University of Regina, Regina, S4S 0A2, Canada
[f] Key Laboratory of Ocean and Marginal Sea Geology, South China Sea Institute of Oceanology, Chinese Academy of Sciences, Guangzhou, 510301, China
[g] Key Laboratory of Metallogenic Prediction of Nonferrous Metals and Geological Environment Monitoring, Ministry of Education, School of Geosciences and Info-Physics, Central South University, Changsha, 410083, China

ARTICLE INFO

Keywords:
Structural reactivation
Late Mesozoic
Gold mineralization
Northeastern Hunan Province
Jiangnan Orogen

ABSTRACT

Gold ore deposits in northeastern Hunan Province are hosted within E-W- to ESE-WNW-trending fracture zones in Neoproterozoic meta-sediments of the Jiangnan Orogen. These rocks have been subjected to multiple tectonic deformations, and the nature of structural control on gold mineralization remains poorly understood. It is unclear when the ore-controlling structures were initially formed and why they are favorable for early Cretaceous gold mineralization. We present a systematic structural analysis to establish a structural evolution model and analyze the structural conditions favorable for gold mineralization. Five deformation events (D_1 to D_5) were identified based on crosscutting and/or overprinting relationships of structural elements. It is established that ore-hosting structures were initially formed during early Paleozoic (D_2), and gold mineralization took place during early Cretaceous (late D_4). The reactivation of D_2 structures during the late D_4 tectonic event, when the stress regime transformed from compression to tension, is critical for gold mineralization. It created a structural network linking mineralizing fluids to structural-chemical traps in Neoproterozoic rocks, where fluid-rock reactions and fluid mixing resulted in gold mineralization. This case study provides a typical example of how structural reactivation played a critical role in mineralization, and emphasizes the significance of structural analysis for mineral exploration.

1. Introduction

Structural reactivation represents temporally separable (intervals >1 Ma) deformation events that repeatedly occur along pre-existing structures such as faults, shear zones, and other geological contacts (Holdsworth et al., 1997, 2001). Many gold deposits around the world occur in ancient structures in Precambrian metamorphic rocks (Kerrich and Cassidy, 1994; Goldfarb et al., 2005; Goldfarb and Groves 2015). The majority of these gold deposits are interpreted to have formed simultaneously with or shortly after the formation of the ore-hosting structures during orogeny, and are therefore termed orogenic gold deposits (Goldfarb et al., 2005). However, many deposits are younger than the initial formation of the ore-hosting structures, such as some of those in the Abitibi greenstone belt in Canada (Sibson et al., 1988), Capricorn Orogen in Western Australia Craton (Miller and Wilson, 2004), Lupa Goldfield (Lawley et al., 2013) and Siguiri Gold District (Lebrun et al., 2017) in Africa, and Qinling Orogen (He et al., 1996), Qinzhou Bay – Hangzhou Bay Juncture Orogen (Jiao et al., 2017) and Jiangnan Orogen (Deng et al., 2020) in Eastern China. This temporal discrepancy between gold mineralization and the initial formation of structures is generally attributed to reactivation of the structures, but the nature of the structural control of mineralization, especially why they were reactivated at the right time and right place that are favorable for gold mineralization, remains poorly understood.

Gold mineralization processes are associated with many factors, including the sources and paths of mineralizing fluids, and

* Corresponding author.
E-mail address: xuderu@gig.ac.cn (D. Xu).

https://doi.org/10.1016/j.jsg.2021.104306
Received 25 December 2020; Received in revised form 8 February 2021; Accepted 9 February 2021
Available online 24 February 2021

physicochemical conditions (pressure, temperature, and fluid composition) favorable for gold precipitation at the sites of mineralization. Among these factors, the paths of mineralizing fluids and sites of mineralization are closely related to structures. Older structures are generally reactivated during subsequent tectonic events if prevailing stress fields are compatible with slip (Dichiarante et al., 2020), since reactivation is mechanically easier than formation of new structures (Sibson, 1985, 2001; Holdsworth et al., 1997). These reactivated structures are commonly more permeable and act as favorable channels for ore fluids (Holdsworth et al., 1997; Li et al., 2019). Fluid-pressure fluctuation (Sibson et al., 1988), variable degrees of weakening (Lawley et al., 2013), and stress field switching (Carrier et al., 2000; Lebrun et al., 2017) during reactivation have also been suggested to be associated with ore precipitation. However, not all structural reactivation results in gold mineralization; structures linking ore-forming fluids with favorable structural-chemical traps play a critical role in mineralization. The role of structural reactivation in gold mineralization is generally complex and requires structural analysis and geochronological – geochemical constraints. Here we provide an example of such analysis from northeastern Hunan Province, in the Jiangnan Orogen in South China.

The Jiangnan Orogen (Fig. 1A) was formed by Neoproterozoic collision between the Yangtze and Cathaysia blocks in South China and underwent poly-deformational events from the early Paleozoic to Mesozoic (Li et al., 2016a; Xu et al., 2017b). It is well-known for its rich gold endowment, with more than 250 gold deposits and occurrences, which contain a total reserve of over 970 tons Au (Xu et al., 2017c; Zhang et al., 2019a). These gold deposits are mostly hosted within fracture zones in Precambrian metamorphic rocks that were initially deformed in the Neoproterozoic (Zhou et al., 1989; Li, 1990; Luo and Chen, 1995; Shu et al., 1995; Luo et al., 1996; Lu et al., 2006; Wu et al., 2006; Huang et al., 2012; Dong, 2014; Xu et al., 2017b), but geochronological data suggest that the mineralization may have occurred from the early Paleozoic to late Mesozoic (Peng et al., 2003; Deng et al., 2017; Xu et al., 2017a; Wang et al., 2019; Zhang et al., 2019b). It remains ambiguous when the structural framework was initially constructed, how it was reactivated during multiple tectonic events, and how structural reactivation was related to gold mineralization.

Among the economically most important gold deposits in the Jiangnan Orogen are the Wangu and Huangjindong gold deposits in northeastern Hunan Province (Fig. 1B), with a reserve of more than 85 and 80 tons of gold respectively (Xu et al., 2017c). Various geochronological methods (including Rb–Sr dating of quartz and associated fluid inclusions, fission-track dating on auriferous quartz, Ar–Ar dating on

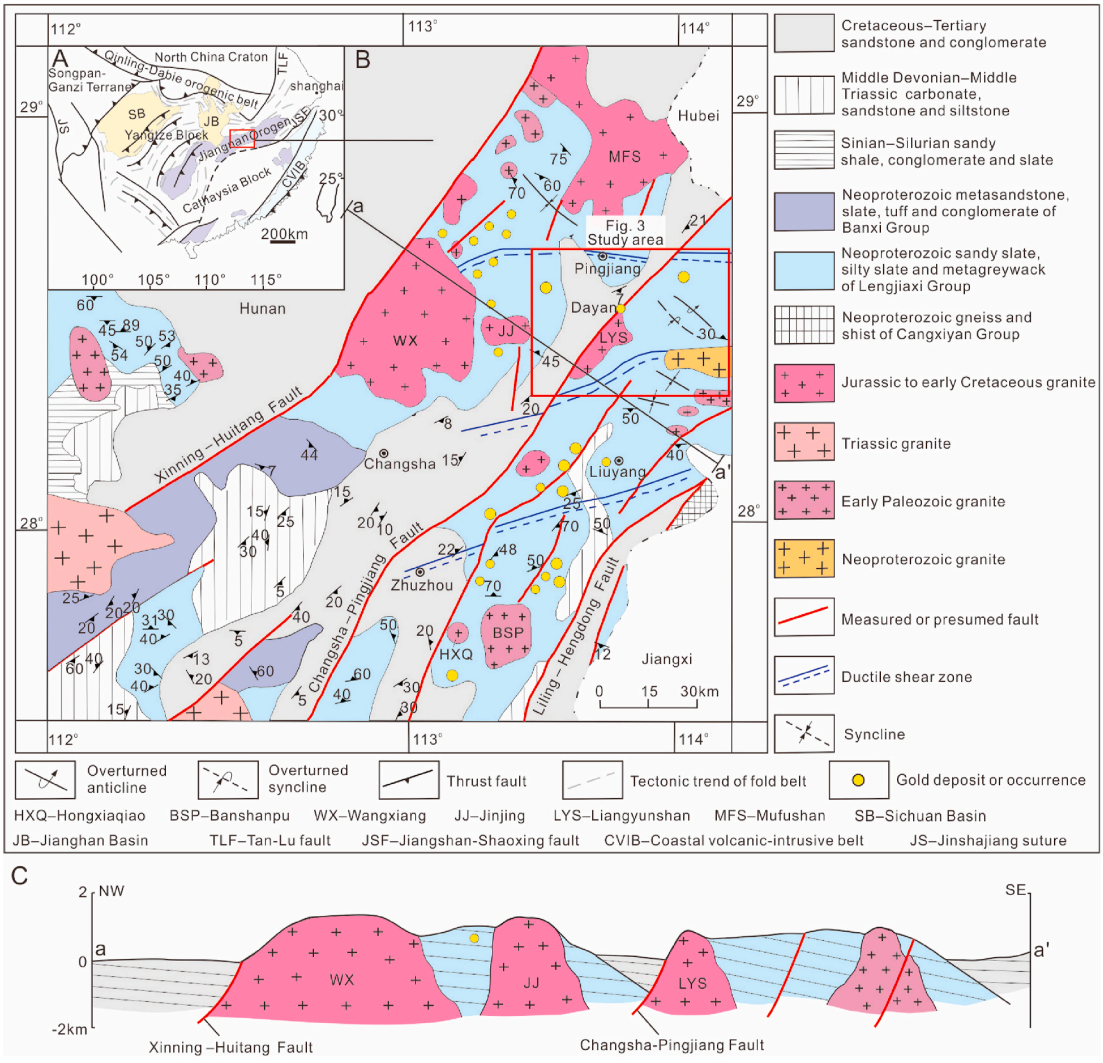

Fig. 1. (A) Simplified tectonic map of the South China block showing location of the Jiangnan Orogen (modified after Ji et al., 2018). (B) Geologic map of northeastern Hunan Province showing distribution of structures, lithologies and major intrusions of different ages, and gold deposits (modified after Xu et al., 2017b). The scope of the study area (Fig. 3) is indicated as a red box; (C) A conceptual NW-SE cross section of northeastern Hunan Province. (For interpretation of the references to colour in this figure legend, the reader is referred to the Web version of this article.)

muscovite and Sm–Nd dating on scheelite) in the Wangu and Huangjindong deposits have yielded various ages ranging from the early Paleozoic (462–400 Ma; Han et al., 2010; Deng et al., 2020) to late Mesozoic (160–70 Ma; Hu et al., 1995; Dong et al., 2008; Deng et al., 2017; Zhou et al., 2020). Some of the most recent studies suggest that the gold mineralization in northeastern Hunan mainly took place in late Mesozoic (Xu et al., 2017b; Deng et al., 2020), but there are several key questions that remain unanswered: When were the ore-hosting structures initially formed? Did mineralization take place at the same time as the initial formation of the ore-hosting structures? If not, when did it happen and why did it occur in these structures? In particular, it remains a puzzle why most of the gold deposits are preferentially hosted in Precambrian rocks, and yet the mineralization is of Mesozoic age. In other words, it is not well understood why gold mineralization did not take place in these structures earlier, and why other structures outside the Precambrian rocks, either initially formed or reactivated in

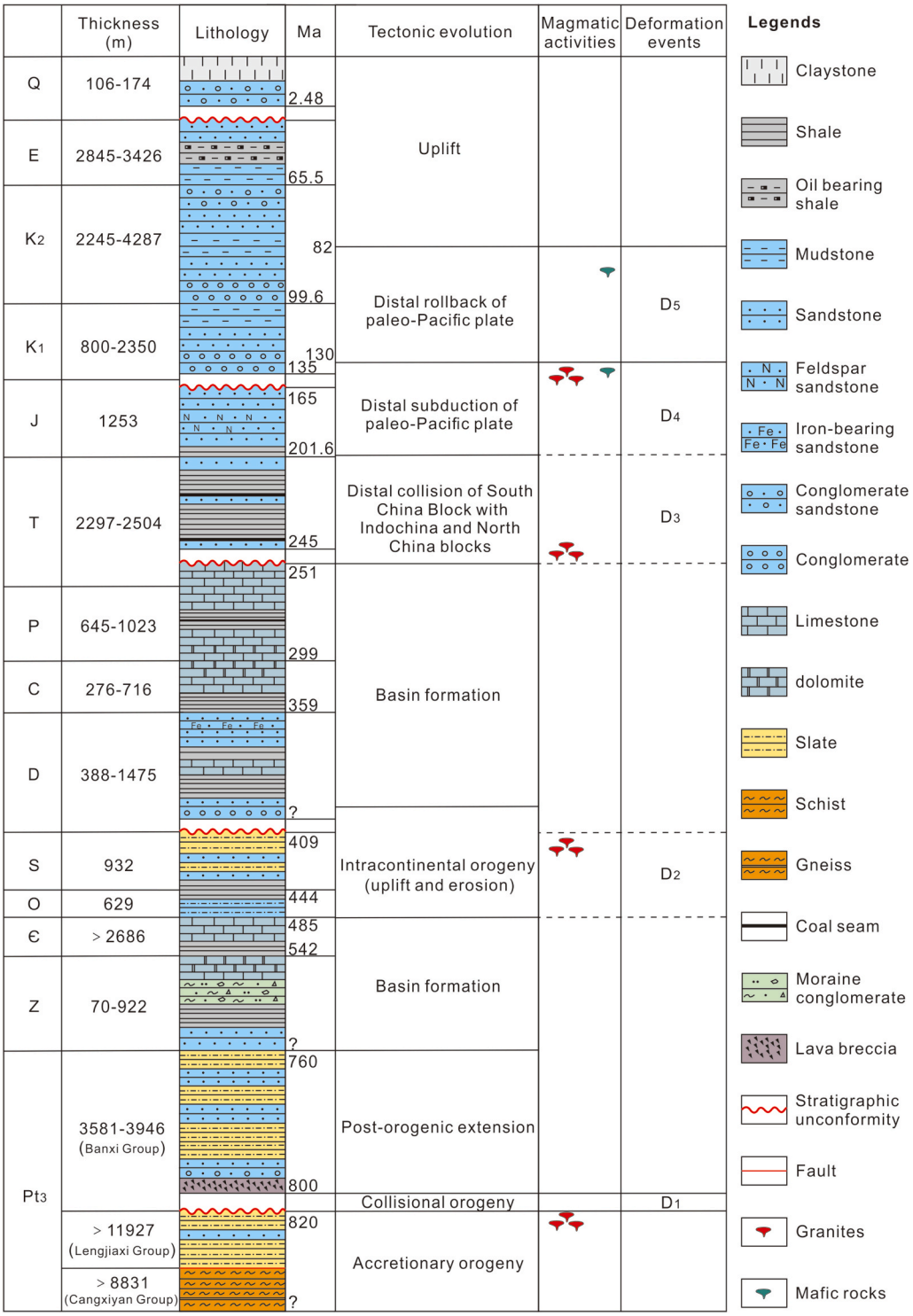

Fig. 2. Stratigraphic column showing lithology, thickness, age of sedimentary and metasedimentary rocks, tectonic evolution, magmatic activities, and deformation events (identified by this study) in northeastern Hunan Province. Modified after Li et al. (2012), Zhang et al. (2019a), and the unpublished internal geologic map of Team 402, Hunan Geology and Mineral Resources Exploration and Development Bureau.

Mesozoic, are less favorable for mineralization.

In order to answer the above questions, we conducted a systematic structural analysis of the northeastern Hunan from Neoproterozoic to late Cretaceous, based on 1:5000 structural observations and measurements in the Wangu and Huangjindong gold deposits and surrounding areas. Different deformation events and related paleostress fields were reconstructed based on kinematic analysis and various overprinting and/or crosscutting relationships observed in the field, in combination with geochronological data obtained by previous studies. The structural evolution model was then used to explain why certain structures formed earlier were more vulnerable for reactivation in later tectonic events, and why some of them are more favorable for gold mineralization, from the perspective of their role in connecting the sources of mineralizing fluids with structural-chemical traps that were favorable for gold precipitation.

2. Geologic setting

2.1. South China block and Jiangnan Orogen

The South China continent comprises two blocks, the Yangtze Block in the northwest and the Cathaysia Block in the southeast. The early Neoproterozoic collision between these two blocks led to the formation of the united South China Block, which made up a part of the supercontinent Rodinia (Charvet et al., 1996; Li et al., 2002, 2007; Ye et al., 2007). The Jiangnan Orogen was created in the southeastern margin of the Yangtze Block (Fig. 1A) and a regional unconformity between the Neoproterozoic Lengjiaxi (> 820 Ma) and Banxi groups (< 800 Ma) was formed during this collision (Fig. 2; Bai et al., 2015; Li et al., 2016a). Rodinia gradually evolved into an extensional regime that eventually resulted in breakup of the supercontinent during the middle to late Neoproterozoic. The Nanhua Rift Basin was formed as a result of this process (Wang and Li, 2003). Sedimentation in the Nanhua Rift Basin started with the Neoproterozoic Banxi Group and lasted until an orogeny in the early Paleozoic (Fig. 1B), which was associated with the closure of the Nanhua Rift Basin (Charvet et al., 2010; Faure et al., 2010) and assembly of Gondwana (Cawood et al., 2017). This orogeny caused uplift and erosion (Charvet et al., 1996; Faure et al., 2010; Li et al., 2016a), and resulted in an angular unconformity between Middle Devonian and Lower Silurian strata (Figs. 1B and 2; Charvet et al., 1996; Sun et al., 2005; Shu et al., 2008).

Since the middle Paleozoic, the South China Block was separated from northern Gondwana during lithospheric extension, drifted northward across the Paleo-Tethys, and subsequently collided with the Asian segment of Pangea (Cawood et al., 2017). This collision spanned the late Permian to late Triassic (early Mesozoic), and caused amalgamation of the South China Block with the Indochina and North China blocks (Wang et al., 2005; Xu et al., 2009b; Zhang et al., 2009; Faure et al., 2010; Li et al., 2014; Shu et al., 2015), which is recorded by widespread intracontinental deformation and a Triassic unconformity (Fig. 2).

The South China Block was affected by the subduction of the Paleo-Pacific plate since early Jurassic (Zhou et al., 2006). It experienced an early stage of shortening in Jurassic and early Cretaceous (Zhou et al., 2006; Shu et al., 2008; Li et al., 2014) and a late stage of extension from late Early Cretaceous to late Cretaceous (ca. 130–82 Ma), which produced a NE-SW-trending basin-and-range-like structural pattern (Figs. 1C and 2; Zhou and Li, 2000; Zhou et al., 2006; Zhang et al., 2012; Li et al., 2014; Li et al., 2016b).

2.2. Regional geology of northeastern Hunan

The northeastern part of Hunan Province, located in the middle segment of the Jiangnan Orogen, is largely occupied by metamorphic Precambrian rocks and unmetamorphosed Cretaceous terrigenous sedimentary rocks. Besides, Paleozoic and Tertiary sedimentary rocks are also present locally (Fig. 1B).

Neoproterozoic, early Paleozoic, early Mesozoic and late Mesozoic magmatic rocks (mainly granitic intrusions) are all present in northeastern Hunan (Figs. 1B and 2). Late Mesozoic, S-type granitoids (ca. 160–130 Ma), are the most widely exposed in the area, mainly occurring along several regional NE-SW-trending faults (Fig. 1B and C;Li, 2006; Wang et al., 2014). More basic rocks dated at ca. 136 Ma and 93–83 Ma also occur in this area (Fig. 2) and show geochemical characteristics similar to OIB, which have been interpreted to reflect asthenosphere upwelling and mixing with crustal materials in an extensional tectonic setting (Jia and Hu, 2002; Jia et al., 2002a, b; Xu et al., 2006).

The Cretaceous to Tertiary sedimentary rocks are distributed in several NE-SW to NNE-SSW-trending rift basins (half grabens). These basins are separated by uplifted basement blocks consisting of granitoids of mainly Mesozoic ages and metamorphic Neoproterozoic rocks, resulting in a basin-and-range like geometry (Fig. 1C). Three approximately E-W-trending ductile shear zones (Fig. 1B) are identified based on geological and geophysical data (Xiao and Chen, 2004). These ductile shear zones have been dated at ca. 450–430 Ma by Ar–Ar dating on muscovite (Li et al., 2016a).

2.3. Characteristics of gold mineralization

There are numerous gold deposits and occurrences in northeastern Hunan Province (Fig. 1B), of which the Wangu and Huangjindong gold deposits are the most productive (more than 165 tons of gold in total; Xu et al., 2017b). These two deposits share similar geological characteristics (Deng et al., 2017, 2020; Xu et al., 2017b) and are both hosted in a suite of Neoproterozoic low-grade metamorphic turbidites of the Lengjiaxi Group, which are composed of sandy and silty slate and metagreywackes (Figs. 1B and 3).

The Wangu gold deposit, with an average grade of 6.8 g/t Au, is arranged in a series of E-W- to ESE-WNW-trending fracture zones dipping moderately to shallowly (60–19°) to north. Ore bodies occur in these fracture zones and are crosscut by NE-SW- to NNE-SSW-trending faults. The ore types include auriferous quartz veins, auriferous altered cataclasite and minor auriferous altered structural breccia (Xu et al., 2017b).

The Huangjindong gold deposit, with grades ranging from 4 to 10 g/t Au (Xu et al., 2017b), is characterized by a series of NW-SE-trending overturned folds and E-W- to ESE-WNW-trending fracture zones. These fracture zones dip to north or south with moderate to shallow dip angles (63–14°). Ore bodies are hosted by these fracture zones and crosscut by NE-SW- to NNE-SSW-trending faults. The ore types are dominated by auriferous quartz veins and auriferous altered cataclasite, with minor auriferous altered structural breccia (Xu et al., 2017b).

3. Methodology

A field survey was conducted in the Wangu and Huangjindong areas to investigate the relationships between gold mineralization and structural deformation (Fig. 3). The geometry and kinematics of folds, faults, cleavages, lineations and veins were observed and measured as in typical structural studies (e.g. Cox et al., 1991) and vein widths and quartz textures were documented (Ortega et al., 2006; Lander and Laubach, 2015). Stress inversion of fault-slip data was done with the software Faultkin (version 7.7.4 by Allmendinger; Angelier, 1984; Marrett and Allmendinger, 1990; Allmendinger et al., 2012). Fault-slip sense of regional faults was inferred from drag folds and subsidiary faults in neighboring outcrops according to the method of Angelier (1994).

Throughout the text, structural events or elements are represented by letters suffixed by numbers to represent the local relative timing of deformation (Williams, 1985). For example, “D” is used for deformation events, while “S” for cleavages, “f” for folds, “L” for lineations and “V” for veins. Thus, S_1 stands for cleavages developed during the D_1 event, and so on.

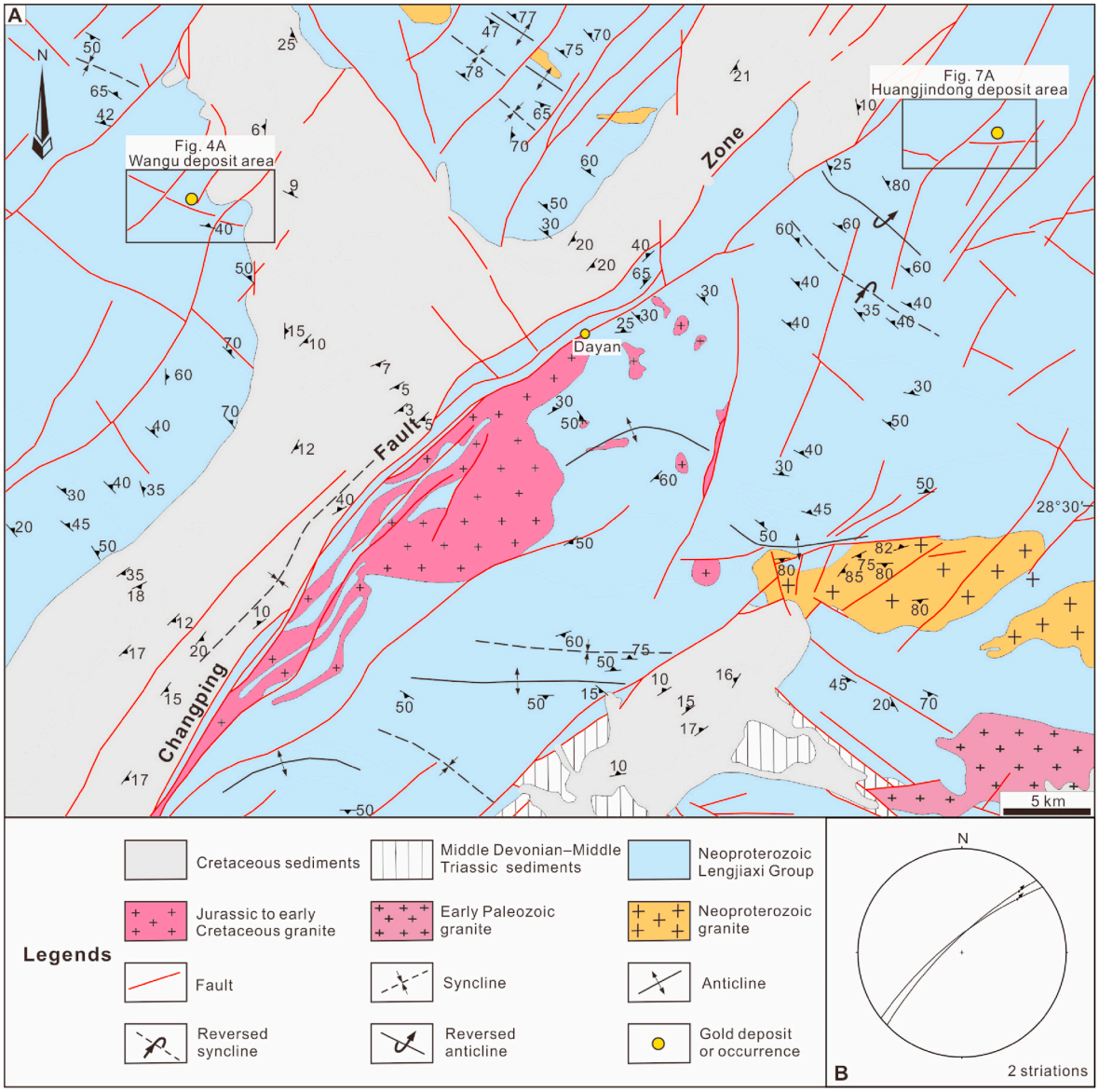

Fig. 3. (A) Geologic map of the study area outlined in Fig. 1B, showing distribution of structures, lithologies and major intrusions of different ages, and the location of the Wangu deposit area (Fig. 4A) and the Huangjindong deposit area (Fig. 7A). (B) Striations on NE-SW-trending subsidiary faults adjacent to the Changping fault zone indicate dextral strike-slip for the Changping fault zone. Stereograms use equal angle (Wulff) projection.

4. Results

4.1. Characteristics of structural deformation

A regional-scale fault zone, the Changsha-Pingjiang (Changping) fault zone traverses the study area (Fig. 1). This fault zone is 60–1100 m wide, 680 km long, strikes NE-SW to NNE-SSW, and dips moderately (70–43°) to NW or WNW (Figs. 1 and 3A). Fault rocks in this fault zone include fault breccias, cataclasites and mylonites. Silicification and gold occurrences occur in the cataclasites. Kinematic indicators suggest multi-phase activities for the Changping fault zone. Drag folds developed in the Neoproterozoic Lengjiaxi Group indicate sinistral strike-slip displacement (Fig. 3A), while striations (defined by quartz fibers) on subsidiary faults suggest dextral strike-slip displacement (Fig. 3B). In addition, syncline and normal faults in the Cretaceous sedimentary rocks indicate normal displacement (Fig. 3A). The Wangu and Huangjindong deposits are located in the hanging-wall and footwall of the Changping fault zone, respectively. The structural characteristics of these two deposits are described using 1:5000 outcrop observations and petrography below.

4.1.1. Wangu deposit area

The Wangu area is located in the northwestern part of the study area, about 16 km from the Changping fault zone (Fig. 3). The Wangu deposit is hosted in sandy slates, silty slates and metagreywackes of the Neoproterozoic Lengjiaxi Group, which is unconformably overlain by Cretaceous sedimentary rocks (Fig. 4A). Two generations of folds, striking NW-SE (f_1) and nearly E-W (f_2) respectively, were recognized in the Lengjiaxi Group by systematic mapping of bedding (Figs. 4A and 5A, C, 6C). Accordingly, two sets of subvertical (90–65°) axial planar cleavages occur in this area, striking NNW-SSE to NW-SE (S_1) (Figs. 4A and 5B) and E-W to ESE-WNW (S_2) (Figs. 4A and 5D) respectively. The S_1 cleavages are crosscut by the S_2 cleavages (Fig. 6B).

The S_2 cleavages are crosscut by a set of subparallel E-W- to ESE-WNW-trending fracture zones dipping moderately to shallowly (60–19°) to the north (Figs. 5E and 6D). These fracture zones are 0.2–14.11 m wide, 200–3280 m long, and extend for more than 2000 m to depth (constrained by drilling). Two generations of striations, defined

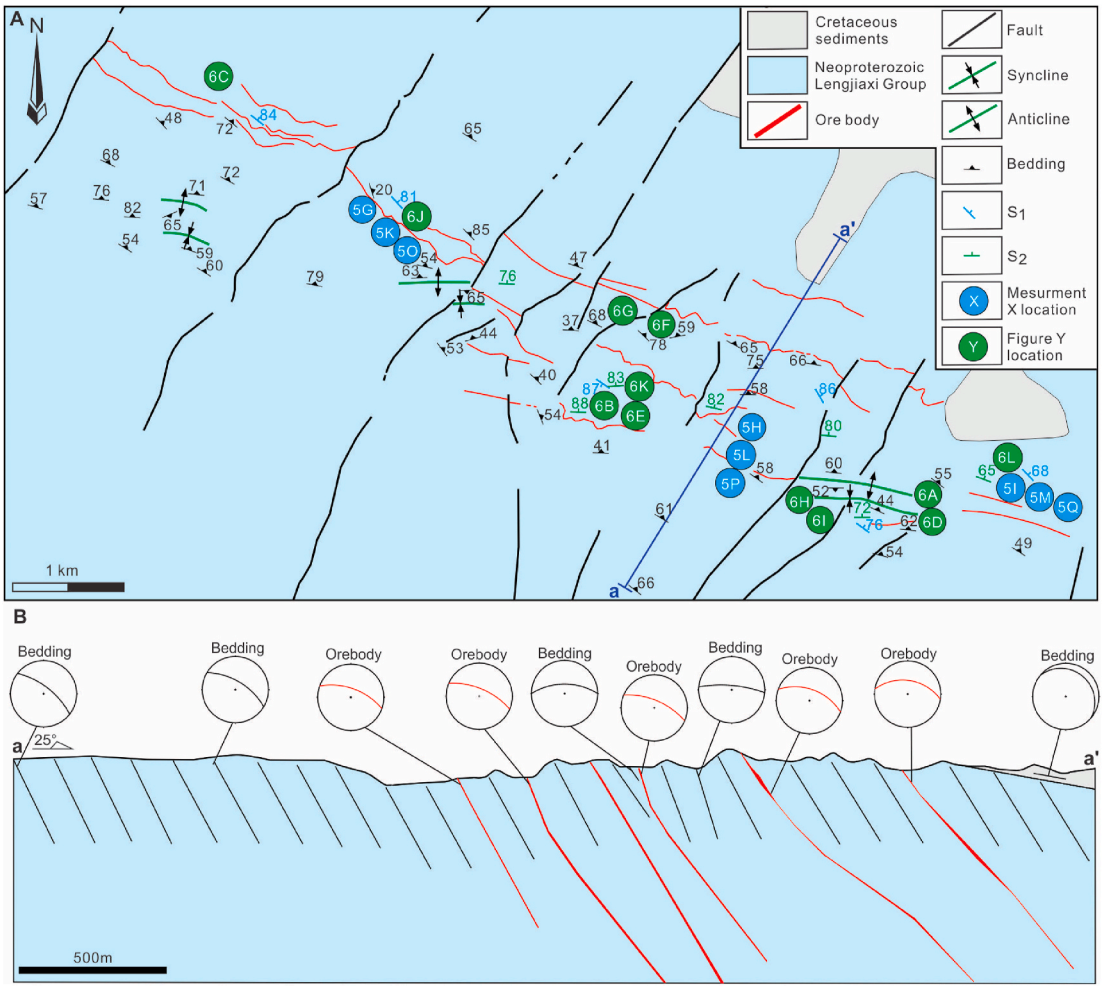

Fig. 4. (A) Geologic map of the Wangu deposit area. (B) A cross section in the Wangu deposit area showing locations of ore bodies. Section line is marked in Fig. 4A.

by quartz fibers or wear grooves, are developed on fault planes of these fracture zones. One generation (L_3) indicates dominant strike-slip displacement with a minor reverse component (Fig. 5G–I, 6H–I), and the other (L_4) crosscuts L_3 striations and indicates dip-slip normal displacement with a minor strike-slip component (Fig. 5K-M, 6H–I). Gold ore bodies in the Wangu deposit, including barren quartz veins and mineralized quartz-pyrite-arsenopyrite veins, are mostly hosted within the E-W- to ESE-WNW-trending fracture zones (Fig. 4A and B).

Multiple sets of quartz veins occur in this deposit area. The oldest veins, indicated by crosscutting relationships, are associated with the second deformation event in this study area and thus termed V_2. V_2 veins include three vein sets. One set is subhorizontal (34–3°) and shows an en echelon geometry along the E-W- to ESE-WNW-trending fracture zones (Figs. 5F and 6F). These veins are developed in extension fractures, 0.1–2.5 cm thick and display a density of ~8 veins/m. Another set of V_2 veins is hosted in E-W- to ESE-WNW-trending shear fractures and dip moderately to shallowly (56–19°) to north or to south. These veins are generally lens-shaped veinlets, 0.2–1 cm thick and were only observed locally, with a density of ~40 veins/m; they crosscut each other and display a conjugate geometry (Fig. 6E). The last set is 1–3 cm thick and developed within S_2 cleavages, with an estimated density of 1 vein every 100 S_2 cleavages (Fig. 6B). The subhorizontal V_2 veins, as well as the S_2 cleavages, are crosscut by a subvertical (86–62°) N–S- to NNW-SSE-trending extension vein set (V_3) (Figs. 5J and 6G, K). The V_3 veins are 0.2–5 cm thick and developed discretely. Both V_2 and V_3 veins are barren, quartz-dominated, and show massive sealing morphologies. Locally, undulose extinction was observed in V_2 and V_3 veins at microscopic scale (Figs. 6M and N).

The V_3 veins are in turn crosscut by approximately E-W-trending extension ore veins (V_4) (Fig. 6K). The V_4 ore veins are 1–10 cm thick and show a density of ~7 veins/m within the E-W- to ESE-WNW-trending fracture zones. They dip either to north or to south at various dip angles (88–5°) and mainly consist of quartz, pyrite and arsenopyrite (Figs. 5N and 6J). The V_4 ore veins show massive sealing morphology, comb structure (Fig. 6O), and crack-seal texture (Fig. 6P). Gold is present as native gold within fractures or invisible gold in arsenopyrite, pyrite, and other sulfides in these ore veins (Deng et al., 2017; Xu et al., 2017b). Locally, another 1- to 10-cm thick extension vein set (V_4), which is dominated by scheelite and quartz, are developed parallel to the V_4 ore veins (Fig. 6L).

The E-W- to ESE-WNW-trending fracture zones and veins (including V_2, V_3 and V_4) therein are both crosscut by numerous equally spaced (average spacing being 1 km) NE-SW- to NNE-SSW-trending normal faults (Fig. 4A; Xu et al., 2017c), suggesting a deformation event post-dating gold mineralization. These NE-SW- to NNE-SSW-trending faults dip steeply to moderately (79–41°) to NW or SE. They are barren, 0.5–20 m wide, and extend for 600–6000 m in length. Fault breccia and fault gouge occur in these faults.

4.1.2. *Huangjindong deposit area*

The Huangjindong **area** is situated in the northeastern part of this study area, about 5 km from the Changping fault zone (Fig. 3). The Huangjindong deposit is hosted in sandy and silty slate of the Lengjiaxi Group and has a structural style characterized by NW-SE-trending

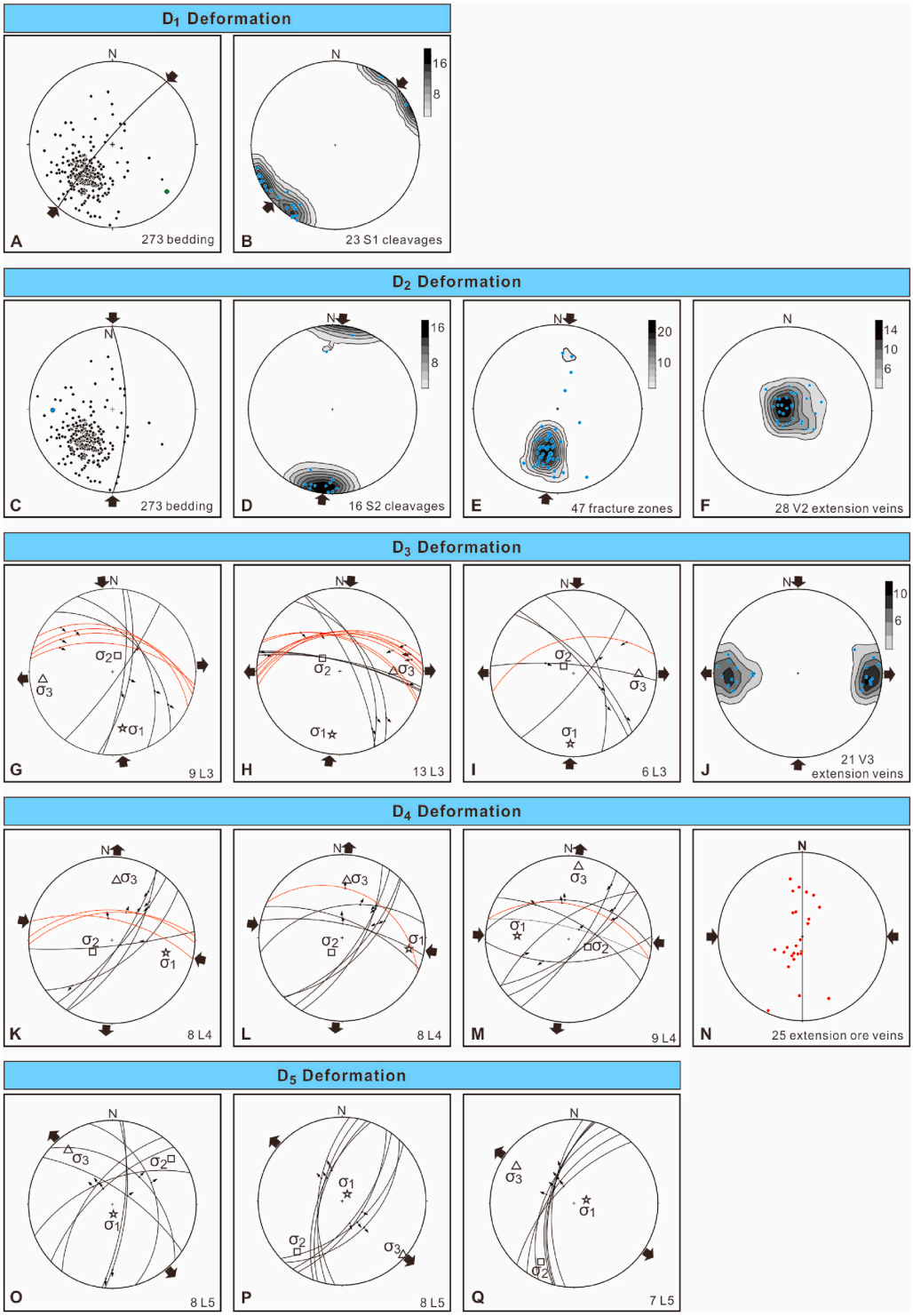

Fig. 5. Stereographic data compilations of structural data from the Wangu deposit area. (A) Poles to bedding of the Neoproterozoic Lengjiaxi Group and constructed great circle and fold axes (in green) for f_1. (B) Poles to NNW-SSE- to NW-SE-trending cleavages (S_1) compatible with a NE-SW contraction (D_1). (C) Poles to bedding of the Neoproterozoic Lengjiaxi Group and constructed great circle and fold axes (in blue) for f_2. (D) Poles to E-W- to ESE-WNW-trending cleavages (S_2) compatible with a N–S contraction (D_2). (E) Poles to ore-hosting fracture zones in the Wangu deposit. (F) Poles to subhorizontal extension veins (V_2) indicating a subvertical σ_3. (G–I) Fault-slip data suggesting a stress field with N–S compression and E-W tension, which characterizes D_3. (J) Poles to subvertical N–S-trending extension veins (V_3) indicating a subhorizontal E-W-trending σ_3. (K–M) Fault-slip data suggesting a stress field with approximately E-W compression and N–S tension, which characterizes D_4. (N) Poles to ore veins in the Wangu deposit suggesting approximately E-W compression with $\sigma_2 \approx \sigma_3$. (O–Q) Fault-slip data suggesting a stress field with NW-SE tension and a subvertical σ_1, which characterizes D_5. Stereograms in Fig. 5B, D-F, and J use lower hemisphere equal area (Schmidt) projection, others use lower hemisphere equal angle (Wulff) projection. Fault-slip data measured on planes of ore-hosting fracture zones are represented by red great circle with black arrows. σ_1, σ_2, and σ_3 represent maximum, intermediate and minimum compressive stresses, respectively. (For interpretation of the references to colour in this figure legend, the reader is referred to the Web version of this article.)

overturned folds (f_1) (Fig. 7A and B, 9A). A NW-SE-trending subvertical (88–61°) axial planar cleavage (S_1) is associated with these folds (Figs. 7A and 8B). The f_1 folds and S_1 cleavages are the oldest structures mapped in this deposit. The f_1 folds are refolded by E-W-trending folds (f_2) (Figs. 7A and 8C), which are linked to E-W- to ESE-WNW-trending subvertical (90–67°) axial planar cleavage (S_2) (Figs. 8D and 9B).

Similar to the Wangu deposit, the E-W- to ESE-WNW-trending cleavages (S_2) are crosscut by E-W- to ESE-WNW-trending fracture zones (Fig. 9C). These fracture zones are 0.46–12.75 m wide, 270–3300 m long along strike, and extend to a depth of more than 1400 m (constrained by drilling). The majority of these fracture zones dips to north and others to south, both with moderate to shallow (63–14°) dip angles. They crosscut each other and show a conjugate geometry (Figs. 8E, 9G-H). Striations (defined by wear grooves), drag folds, and structural geometries suggest that they have experienced reverse (Fig. 9C), strike-slip (Fig. 9E), and normal displacements (Fig. 9F). Gold ore bodies are mostly hosted in these E-W- to ESE-WNW-trending fracture zones (Fig. 7A and B).

The oldest veins (V_2) at Huangjindong, identified based on crosscutting relationships, are subdivided into two vein sets. The first set is

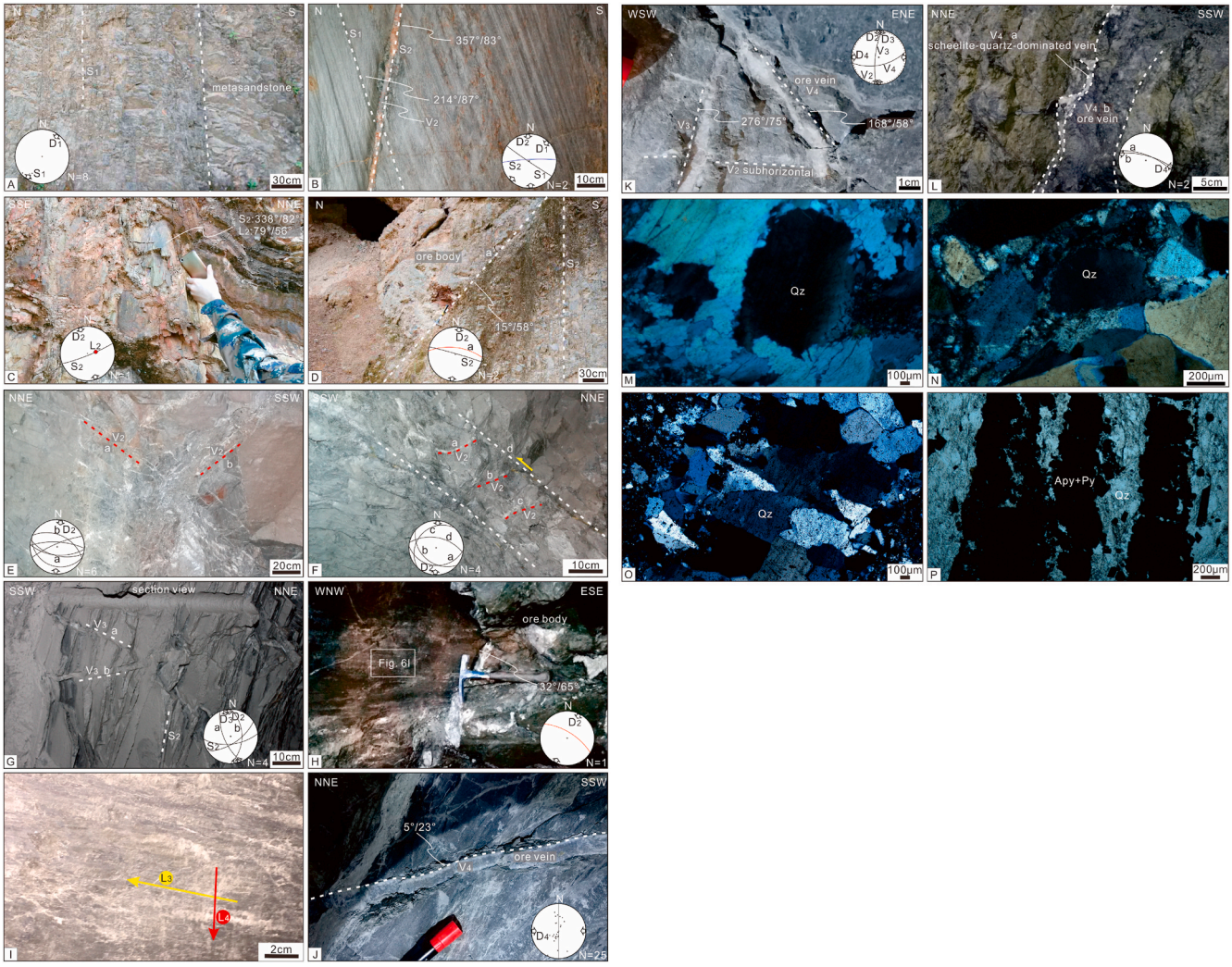

Fig. 6. Field photographs from the Wangu deposit. (A) Subvertical NW-SE-trending cleavages (S_1) occurring in metasandstones. (B) Subvertical NW-SE-trending cleavages (S_1) crosscut by subvertical E-W-trending ones (S_2). (C) A meso-scale fold (f_2) with subvertical ENE-WSW-trending axial plane. (D) Subvertical WNW-ESE-trending cleavages (S_2) crosscut by ore-hosting E-W-trending fracture zones. (E) Barren E-W- to ESE-WNW-trending quartz veins (V_2) showing a conjugate geometry. (F) Subhorizontal barren quartz veins (V_2) occurring in a reverse fracture zone. (G) Subvertical E-W- to ENE-WSW-trending cleavages (S_2) crosscut by steeply to moderately dipping N–S-trending barren quartz veins (V_3). (H and I) L_3 and L_4 striations on the same fault planes of ore-hosting fracture zone. Note the striations linked to D_3 are overprinted by those linked to D_4. (J) An auriferous quartz vein characterized by mineral assemblage of quartz, pyrite and arsenopyrite, termed ore vein. (K) Crosscutting relationships between subhorizontal barren quartz vein (V_2), subvertical barren quartz vein (V_3), and approximately E-W-trending ore vein (V_4). Note that V_3 crosscuts V_2 and is in turn crosscut by V_4. (L) A WNW-ESE-trending scheelite-quartz-dominated vein (V_4) accompanying ore vein (V_4) with similar orientation. (M–N) V_2 (M) and V_3 (N) barren quartz veins showing undulose extinction. (O–P) Auriferous quartz-pyrite-arsenopyrite veins (V_4) showing comb structure (O) and crack-seal texture (P). (M–P) are taken under crossed-polarized light. Abbreviations: Apy, arsenopyrite; Py, pyrite; and Qz, quartz.

0.8–4 cm in thickness and hosted in subhorizontal (28–5°) extension fractures which display an intensity of ~8 fractures/m (Figs. 8F and 9K). The second vein set is 1–2.2 cm thick and developed within S_2 cleavages (about 1 vein every 50 S_2 cleavages) (Fig. 9B). The V_2 veins are crosscut by a set of subvertical (87–56°) N–S-trending extension veins (V_3), which are developed simultaneously with minor reverse displacement (interpreted to be associated with strike-slip displacement with minor reverse component; see section 4.2) along E-W- to ESE-WNW-trending faults (Figs. 8J and 9I, K). The V_3 veins are 1–45 cm thick. Both V_2 and V_3 veins are barren, quartz-dominated, and show massive sealing morphologies. In thin section, they display undulose extinction in places (Figs. 9O and P).

The N–S-trending veins (V_3) are crosscut by E-W- to ESE-WNW- and ENE-WSW-trending extension ore veins (V_4) associated with normal faulting (Fig. 9I and K). These ore veins are generally 0.2–2.5 cm thick and display densities as high as 83 veins/m locally. Dip angles of these veins vary from 73° to 26° (Fig. 8N). The V_4 ore veins are mainly composed of quartz, pyrite, and arsenopyrite (Fig. 9J). Native gold occurs within fractures in arsenopyrite, while invisible gold mainly occurs in arsenopyrite and pyrite in these ore veins (Liu et al., 1989). The V_4 ore veins show massive sealing morphologies, with comb structure (Fig. 9Q) and crack-seal texture (Fig. 9R) observed locally. A vein set (V_4) dominated by scheelite and quartz is also present in places. These scheelite-quartz veins are generally 1–8 cm thick, accompanied by the ore veins, and show similar orientations to the ore veins (Fig. 9L).

Gold ore bodies at Huangjindong, as well as the ore-hosting E-W- to ESE-WNW-trending fracture zones, are crosscut by a series of NE-SW-trending normal faults (Figs. 7A and 9M). These NE-SW-trending faults mainly dip moderately (65–36°) to NW, minor to SE. They are not mineralized, 0.2–10 m wide, and extend as long as 5000 m along strike. Fault gouges and fault breccias are developed in these faults. Striations (L_5) defined by wear grooves are present on these faults (Fig. 9N) and are associated with NW-SE extension, indicating an extensional event after gold mineralization (Fig. 8O–Q).

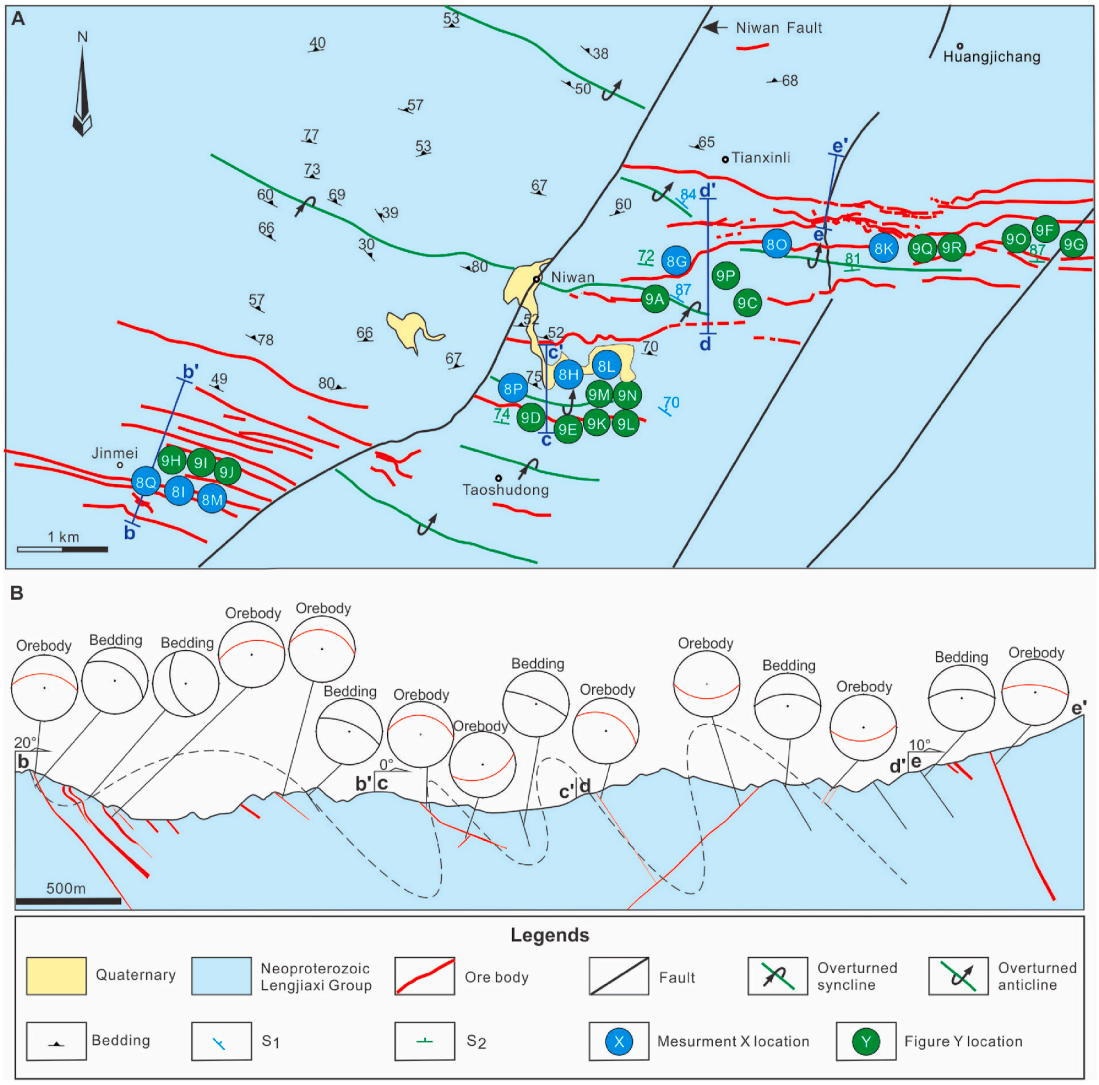

Fig. 7. (A) Geologic map of the Huangjindong deposit area (modified after Xu et al., 2017b). (B) A cross section in the Huangjindong deposit area showing the location of ore bodies (see Fig. 7A for its location).

4.2. Sequence of deformation and paleostress analysis

Based on overprinting and crosscutting relationships, the structural elements documented above are grouped into five deformation events, labelled D_1 to D_5. D_1 to D_4 were only observed in the Neoproterozoic Lengjiaxi Group, while D_5 was observed in both the Neoproterozoic Lengjiaxi Group and the Cretaceous sedimentary rocks (Fig. 10). The characteristics of individual deformation events and their relationships with each other, including reactivation of pre-existing structures, as well as their relationships with gold mineralization, are described below.

D_1-deformation: As the earliest deformational epoch observed in this study area, D_1 is a ductile event characterized by folds (f_1) and cleavages (S_1) (Fig. 10A). The f_1 folds are mainly NW-SE-trending but locally WNW-ESE-trending (Figs. 5A, 7A and 8A). Remnants of these folds were observed locally in the Huangjindong area (Fig. 9A). The S_1 cleavages generally strike NW-SE and mostly dip steeply (90–61°) to NE (Figs. 4A, 5B and 7A, 8B).

Folds and cleavages developed in incompetent sedimentary rocks between two blocks are commonly parallel to the boundary of competent blocks (Wang, 2010; Bai et al., 2012). As documented by Bai et al. (2012), the oldest structures (i.e., folds and cleavages) in the Neoproterozoic Lengjiaxi Group in the Jiangnan Orogen are NE-SW-trending in the southwestern segment but E-W-, WNW-ESE- and NW-SE-trending in the middle segment, apparently controlled by the morphology of the boundary between the Yangtze and Cathaysia blocks. The NW-SE-trending folds (f_1) and cleavages (S_1) in this study area (the middle segment of the Jiangnan Orogen; Fig. 1A) are associated with the first deformation event since the formation of the Lengjiaxi Group and are parallel to the competent boundary of the Yangtze block to the northwest. Therefore, they are interpreted to be caused by the Neoproterozoic (ca. 820–800 Ma) collision between the Yangtze and Cathaysia blocks under a regional NW-SE shortening (Figs. 2 and 10A; Cawood et al., 2017). The regional, deep Changping fault zone may have been initiated at this time (Fig. 10A).

D_2-deformation: Structural elements associated with the second deformation event are dominated by early-stage folds (f_2) and associated cleavages (S_2), and late-stage E-W- to ESE-WNW-trending fracture zones and barren quartz veins (V_2) (Fig. 10B). S_2 cleavages crosscut S_1 cleavages (Fig. 6B) and are in turn crosscut by the E-W- to ESE-WNW-trending fracture zones (Figs. 6D and 9C).

The f_2 folds have axes generally striking E-W and plunging shallowly (20–10°) to west and east in the Wangu and Huangjindong area, respectively (Figs. 5C and 8C). Associated axial planar cleavages (S_2) strike E-W- to ESE-WNW and dip steeply (90–65°) to north or south (Figs. 4A, 5D and 6B, G, 7A, 8D).

The geometry of E-W- to ESE-WNW-trending fracture zones and the

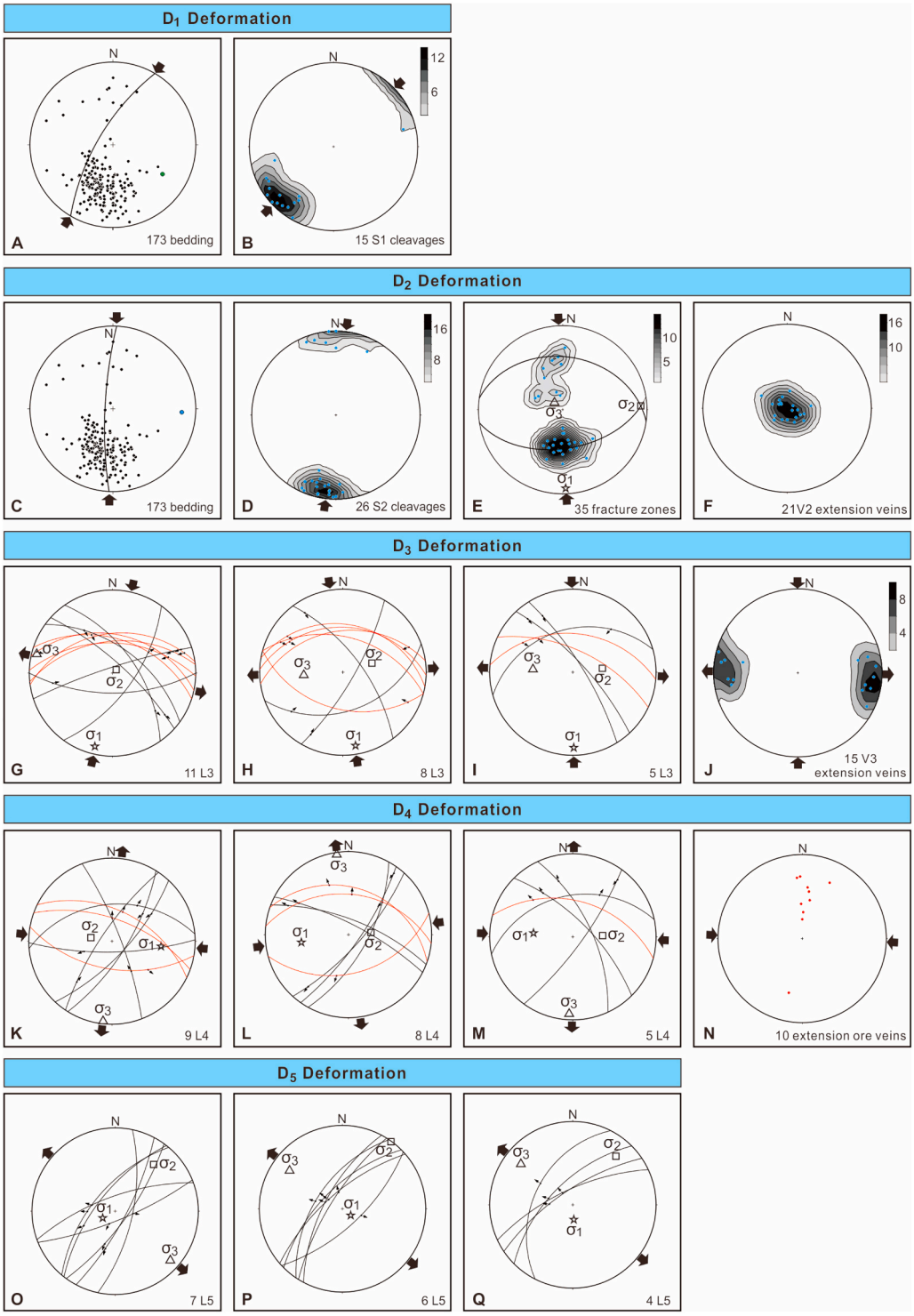

Fig. 8. Stereographic data compilations of structural data from the Wangu deposit area. (A) Bedding poles measured in the Lengjiaxi Group and constructed great circle and fold axes (in green) for f_1. (B) Poles to NW-SE-trending cleavages (S_1) associated with NE-SW contraction (D_1). (C) Bedding poles measured in the Lengjiaxi Group and constructed great circle and fold axes (in blue) for f_2. (D) Poles to E-W- to ESE-WNW-trending cleavages (S_2) linked to N–S contraction (D_2). (E) Poles to ore-hosting fracture zones in the Huangjindong deposit. (F) Poles to subhorizontal extension veins (V_2) indicating a subvertical σ_3. (G–I) Fault-slip data suggesting N–S compression and E-W tension characterizing D_3. (J) Poles to subvertical N–S-trending extension veins (V_3) indicating a subhorizontal E-W-trending σ_3. (K–M) Fault-slip data suggesting approximately E-W compression and N–S tension characterizing D_4. (N) Poles to ore veins in the Huangjindong deposit. (O–Q) Fault-slip data suggesting NW-SE tension accompanied by a subvertical σ_1 which characterizes D_5. Stereograms in Fig. 8B, D-F, and J use lower hemisphere equal area (Schmidt) projection, others use lower hemisphere equal angle (Wulff) projection. Fault-slip data measured on planes of ore-hosting fracture zones are represented as red great circles with black arrows. σ_1, σ_2, and σ_3 represent maximum, intermediate and minimum compressive stresses, respectively. (For interpretation of the references to colour in this figure legend, the reader is referred to the Web version of this article.)

development of subhorizontal veins (V_2) reflect an approximate N–S compression with a vertical σ_3 (Fig. 5E and F, 6E, F, 8E, F). This stress field is compatible with the early-stage folds (f_2) (Figs. 5C and 8C) and cleavages (S_2) (Figs. 5D and 6B, G, 8D) in this study area, as well as the approximately E-W-trending folds in pre-Devonian basement in the South China Block which have been interpreted to be associated with the early Paleozoic orogeny (Qiu et al., 1998; Chen and Rong, 1999; Qiu, 1999; Hao et al., 2010; Bai et al., 2012). As such, the ~E-W-trending folds, S_2 cleavages, E-W- to ESE-WNW-trending fracture zones, and V_2 veins in this study area are interpreted to be formed during the early Paleozoic. A switch from ductile-to brittle deformation during the D_2 event, indicated by the change of structural styles from the early to late stage, probably resulted from the uplift and erosion linked to the early Paleozoic orogeny (Fig. 2; Charvet et al., 1996; Faure et al., 2010; Li et al., 2016a). This is further supported by Ar–Ar dating (ca. 400 Ma; Deng et al., 2020) on muscovite crosscutting barren veins within the E-W- to ESE-WNW-trending fracture zones in the Huangjindong deposit. This tectonic regime may have caused sinistral strike-slip displacement along the Changping fault zone, which is consistent with drag folds in the Neoproterozoic Lengjiaxi Group (Figs. 3A and 10B).

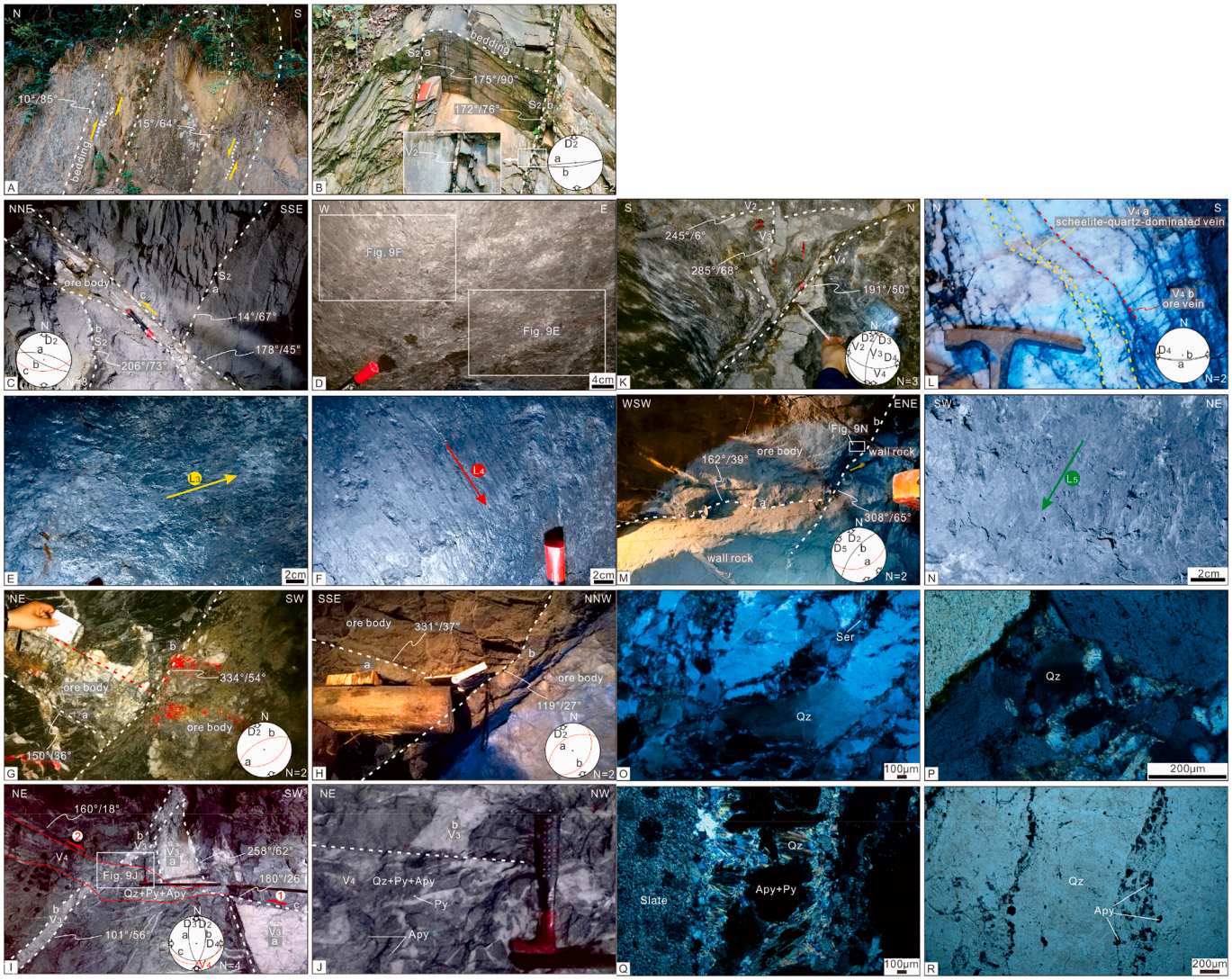

Fig. 9. Field views from the Huangjindong deposit. (A) WNW-ESE-trending overturned anticline (f_1) developed in the Lengjiaxi Group. (B) E-W-trending folds (f_2) and associated E-W-trending subvertical axial planar cleavages (S_2). Note these cleavages are locally filled with barren quartz veins (V_2). (C) WNW-ESE-trending cleavages (S_1) crosscut by an E-W-trending ore-hosting fracture zone. (D–F) Two sets of striations (L_3 and L_4) suggesting strike-slip (E) and normal faulting (F) occur on the roof of an E-W-trending ore-hosting fracture zone (D). (G and H) Two sets of ENE-WSW-trending ore-hosting fracture zones with mutual crosscutting relationship. (I and J) N–S-trending barren quartz veins (V_3) crosscut by a fault showing an early reverse displacement and a later normal displacement. Note auriferous quartz-pyrite-arsenopyrite veins (V_4) are associated with normal displacement of the ENE-WSW-trending fault. (K) Crosscutting relationships of sub-horizontal barren quartz vein (V_2), subvertical barren quartz vein (V_3), and nearly E-W-trending auriferous quartz vein (V_4). Note that V_2 is crosscut by V_3 while both of them are crosscut by V_4. (L) Scheelite veins (V_4) showing similar orientations to ore veins (V_4). (M and N) A nearly E-W-trending gold ore body is crosscut by an NE-SW-trending fault (M), which bears striations (L_5) indicating NW-SE tension linked to D_5-deformation (N). (O) V_2 barren quartz veins showing undulose extinction with sericite occurring in cracks. (P) V_3 barren quartz veins showing undulose extinction. (Q–R) Auriferous quartz-pyrite-arsenopyrite veins (V_4) showing comb structure (Q) and crack-seal texture (R). (O–R) are taken under crossed-polarized light. Abbreviations: Apy, arsenopyrite; Py, pyrite; Qz, quartz; and Ser, sericite.

D_3-deformation: This event is manifested as veins (V_3) and faults in the Neoproterozoic Lengjiaxi Group (Fig. 10C). D_3-deformation is inferred to postdate D_2-deformation based on crosscutting relationship of S_2 (early D_2-deformation) and V_2 (late D_2-deformation) by V_3 (e.g., at Wangu and Huangjindong; Fig. 6G, K, 9K).

The L_3 striations imply a paleostress field with N–S compression and E-W tension (Fig. 5G–I, 8G-I), compatible with the geometries of V_3 veins (Figs. 5J and 8J). The Changping fault zone might be subject to sinistral strike-slip displacement under this stress regime, which is indicated by drag folds in the Neoproterozoic Lengjiaxi Group (Figs. 3A and 10C). Although both D_2-and D_3-deformations are linked to N–S compression, the tensional stress (i.e., σ_3) is subvertical during D_2-deformation, but subhorizontal during D_3-deformation.

Despite lack of geochronological evidence, this reconstructed stress

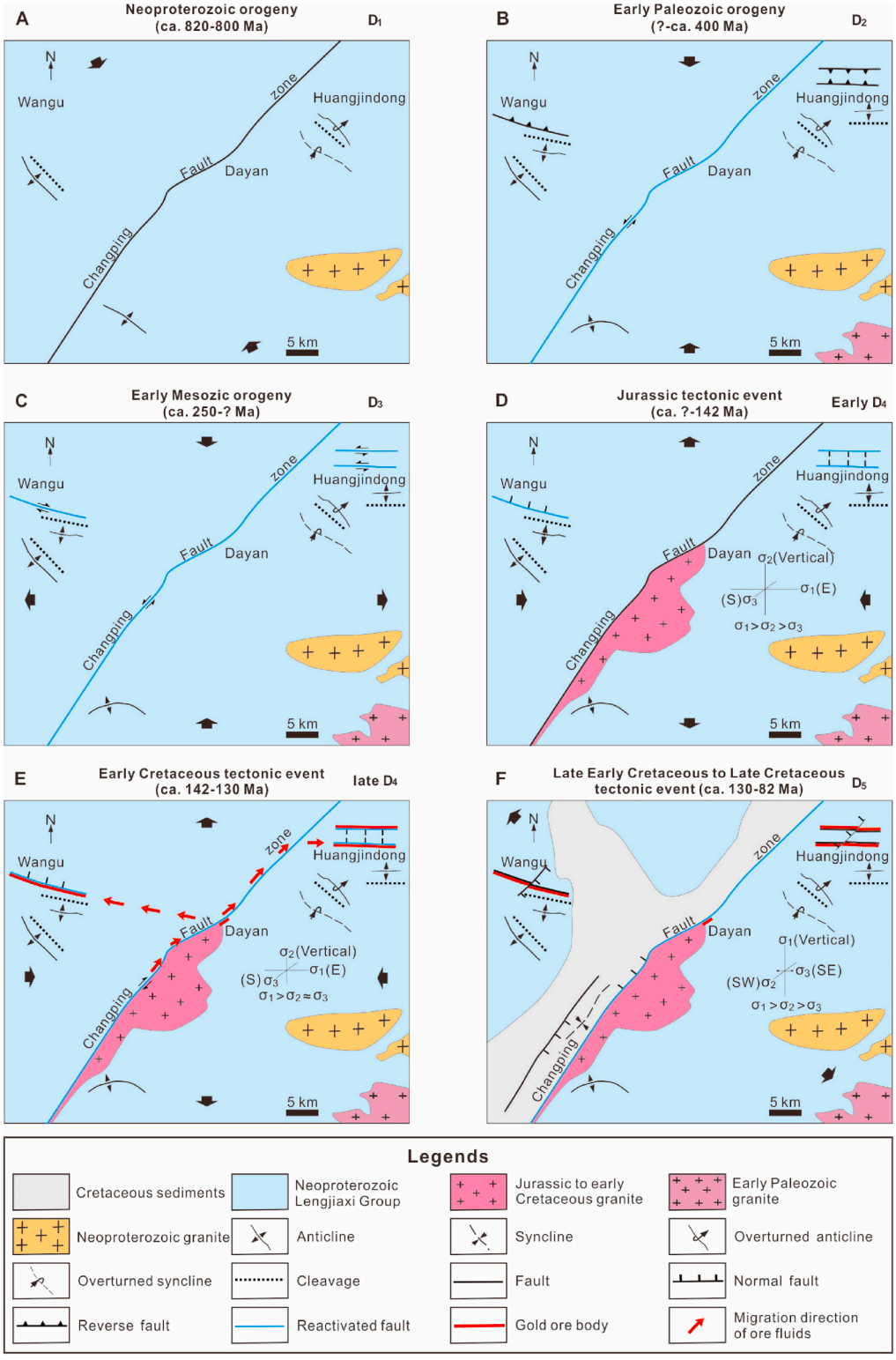

Fig. 10. Sketch maps showing evolution of structural elements, stress field through multiple tectonic events (from D_1 to D_5-deformation) and their relationship with gold mineralization in northeastern Hunan Province. Scale is approximate.

field is compatible with the structural elements associated with the early Mesozoic orogeny in the South China Block, which occurred in an intracontinental tectonic setting since ca. 250 Ma and are characterized by E-W- to ESE-WNW-trending folds, and NE-SW- to NNE-SSW-trending sinistral strike-slip faults (Fig. 2; Wang et al., 2005; Xu et al., 2009b; Zhang et al., 2009; Shu et al., 2015). Consequently, D_3-deformation is considered to be generated by this orogeny. The N–S compression probably stemmed from the collision of the South China Block with the North China to the north and Indochina Blocks to the southwest (Faure et al., 2014).

D_4-deformation: The structural styles associated with the deformation event include ore veins (V_4), scheelite-quartz veins (V_4) and faults in the Lengjiaxi Group (Fig. 10D and E). In the Wangu and Huangjindong deposits, striations (L_3) formed during D_3-deformation

are overprinted by those (L_4) developed during D_4-deformation (Figs. 6I and 9D), and N–S-trending subvertical barren veins (V_3) are crosscut by ~ E-W-trending ore veins (V_4) (Figs. 6K and 9I-K). All these overprinting and crosscutting relationships suggest that D_4-deformation is a deformation event postdating D_3-deformation.

As the orientation of σ_3 corresponds to the pole of the planes representing veins on stereographic diagrams (Miller and Wilson, 2004b), the variable opening directions for the V_4 ore veins indicate an uniaxial E-W compression with $\sigma_2 \approx \sigma_3$ (Figs. 5N and 8N). This E-W compression is compatible with L_4 striations (Fig. 5K-M, 8K-M), which were partly observed on fault planes of the ore-hosting E-W- to ESE-WNW-trending fracture zones and indicate normal movement sense (Figs. 6I and 9F). The Changping fault zone possibly underwent dextral shear under this stress regime (Fig. 10D and E), which is indicated by striations on subsidiary faults in adjacent outcrops (Fig. 3B).

This stress regime is also compatible with the numerous NE-SW- to NNE-SSW-trending folds and thrust structures in the South China Block, which have been interpreted to be formed during the Jurassic to early Cretaceous tectonic event (Fig. 2; Xu et al., 2009b; Li et al., 2014). Moreover, the ore veins (V_4) and scheelite-quartz veins (V_4) have been constrained to 142–130 Ma (Deng et al., 2017) and 129.7 Ma (Zhou et al., 2020), respectively. Hence, D_4-deformation was probably caused by the subduction of the Paleo-Pacific plate beneath the South China Block during the Jurassic to early Cretaceous tectonic event (Zhou et al., 2006).

D_5-deformation: This deformation event is indicated by normal faults in both the Neoproterozoic Lengjiaxi Group and the Cretaceous sedimentary rocks. Ore bodies composed of V_2 (barren quartz veins), V_3 (barren quartz veins) and V_4 (ore veins and scheelite-quartz veins) are crosscut by NE-SW- to NNE-SSW-trending faults bearing L_5 striations (Figs. 4A, 7A, 9M-N), indicating that D_5-deformation postdates D_4-deformation.

The D_5 structural characteristics, especially L_5 striations, suggest NW-SE tension with a vertical σ_1 (Li et al., 2016a, Fig. 5O–Q, 8O-Q). This is consistent with the late Early Cretaceous to late Cretaceous (ca. 130–82) stress regime which has been interpreted to be caused by the rollback of the Paleo-Pacific slab and have produced a NE-SW-trending basin-and-range-like structural pattern in the South China Block (Fig. 2; Zhou and Li, 2000; Zhou et al., 2006; Zhang et al., 2012; Li et al., 2016b). The regional NE-SW-trending Changping fault zone may have experienced normal movement under this stress regime, as indicated by drag folds (syncline) and normal faults in the Cretaceous sedimentary rocks in its northwest (Figs. 3A and 10F).

5. Discussion

The gold deposits in northeastern Hunan Province are mainly hosted in the E-W- to ESE-WNW-trending fracture zones within the Neoproterozoic Lengjiaxi Group. These fracture zones have been considered to be initially formed before the late Mesozoic (Fig. 2; Xu et al., 2017c), but the actual timing has been uncertain. Wen et al. (2016) suggested that these fracture zones were formed during the early Paleozoic or early Mesozoic orogeny, as the geometries of the E-W- to ESE-WNW-trending fracture zones are associated with N–S compression during these orogenies. However, Fu et al. (1999) interpreted the E-W- to ESE-WNW-trending fracture zones to be formed during the early Paleozoic or Neoproterozoic orogeny, because they are overprinted by early Mesozoic structures. This argument is also supported by the occurrence of quartz veins older than 400 Ma within the E-W- to ESE-WNW-trending fracture zones (Deng et al., 2020). In addition, the E-W- to ESE-WNW-trending fracture zones truncate the E-W- to ESE-WNW-trending cleavages (S_2) (Figs. 6D and 9C), which in turn crosscut the NW-SE-to NNW-SSE-trending cleavages (S_1) associated with the Neoproterozoic orogeny (Fig. 6B). This indicates that the E-W- to ESE-WNW-trending fracture zones postdate the Neoproterozoic deformation and were formed during the early Paleozoic orogeny (Fig. 2). The geometries (Figs. 5E and 8E) and ductile-to-brittle structural characteristics (see section 4.2) of the E-W- to ESE-WNW-trending fracture zones are also consistent with the early Paleozoic orogeny (Charvet et al., 1996; Qiu et al., 1998; Chen and Rong, 1999; Qiu, 1999; Faure et al., 2010; Hao et al., 2010; Li et al., 2016a).

The timing of gold mineralization has also been controversial, with opinions ranging from early Paleozoic (Han et al., 2010) to late Mesozoic (Hu et al., 1995; Dong et al., 2008; Deng et al., 2017; Zhou et al., 2020) orogenies. The late Mesozoic ages are believed to be more plausible based on the following considerations. First, the early Paleozoic ages (ca. 462 Ma and 425 Ma; Han et al., 2010), which were obtained from Rb–Sr dating of quartz and associated fluid inclusions, may not be directly related to the age of mineralization due to the nature of the analysis (bulk fluid inclusions). Second, quartz veins (V_2) that are constrained to the early Paleozoic (>400 Ma) by Ar–Ar dating on muscovite (Deng et al., 2020) and vein geometries (Figs. 5F and 8F) are all barren. Finally, quartz veins (V_3) that are constrained to the early Mesozoic by vein geometries (Figs. 5J and 8J) are also barren. Thus, the age of gold mineralization, which is closely associated with V_4 veins, is likely post-early Mesozoic. Some of the late Mesozoic ages obtained from Rb–Sr dating of quartz and associated fluid inclusions (152 Ma and 70 Ma; Dong et al., 2008) and fission-track dating on quartz (160–115 Ma; Hu et al., 1995), which were proposed to represent gold mineralization ages, were too broad to be useful. However, a few more recent geochronological studies on Sm–Nd dating of scheelite (Zhou et al., 2020) and Ar–Ar dating of muscovite (Deng et al., 2017) associated with V_4 veins were able to constrain the gold mineralization ages to ca. 142–130 Ma. This age interval is consistent with the structural and stress analysis that indicates D_4 deformation event and V_4 formation took place in the Jurassic to early Cretaceous (Fig. 10).

It is remarkable to note that both barren veins formed in the early Paleozoic and early Mesozoic orogenies and auriferous veins formed in the Jurassic to early Cretaceous tectonic events are controlled by the same E-W- to ESE-WNW-trending fracture zones. Since these structures were initially formed in the early Paleozoic, it follows that gold mineralization was related to reactivation of these structures. Structural reactivation has been shown to be controlled by the orientations of pre-existing structures, differential stress, fluid pressure, and friction coefficient (Sibson, 1985, 2001). Favorably oriented structures are easy to be reactivated, while others require more demanding conditions such as relatively low differential stress level in combination with high fluid pressure (Sibson, 1985). Effective principal stresses, which are principal compressive stresses minus fluid pressure, are among the most important factors controlling faulting and fracturing. Buildup of fluid pressure generally pushes the Mohr stress circle towards left and induces reactivation (Sibson et al., 1988), and low friction coefficient is also favorable for structural reactivation (Sibson, 1985). It has been widely accepted that pre-existing structures represent structural weakness, with tensile strength (T) approaching zero (Sibson, 1985). Consequently, reactivation of pre-existing structures commonly occurs in preference to the formation of new faults in a new round of deformation (Sibson, 1985, 2001). Indeed, the E-W- to ESE-WNW-trending fracture zones and the regional NE-SW-trending Changping fault zone in northeastern Hunan Province may have been reactivated multiple times since they were formed (Fig. 10).

A question that follows from the above discussions is why the ore-hosting structures, which were initially formed in the early Paleozoic orogeny, were not mineralized until early Cretaceous (ca. 142–130 Ma). The absence of gold mineralization during the early Paleozoic and early Mesozoic may be related to many factors, including lack of ore fluids and/or lack of structures connecting the ore fluids with the ore-hosting structures. Based on fluid inclusion data, H–O, He–Ar and S–Pb isotopes, and regional geological setting, it has been proposed that the ore-forming fluids for gold mineralization in northeastern Hunan may have been derived from various sources including metamorphic, magmatic and mantle-derived fluids (Mao et al., 1997; Mao and Li,

1997; Mao et al., 2002; Li et al., 2011; Deng et al., 2017, 2020). The ore fluids may have been developed as mixtures of fluids from different sources and stored at depth in the upper crust. No gold mineralization would occur until the ore fluids were tapped by deep structures and drained to structures suitable for ore precipitation. The connection between the E-W- to ESE-WNW-trending fracture zones and ore fluid sources has been interpreted to be associated with a change of these fracture zones from contraction to extension (Xiao et al., 2002; Xiao and Chen, 2004; Xu et al., 2017c), which is supported by the structural analyses presented in this study. However, the change of the E-W- to ESE-WNW-trending fracture zones from contraction to extension does not necessarily lead to gold mineralization, because these shallow-dipping structures could hardly reach the ore fluids at depth.

Here we propose that the ore fluids were tapped by the Changping fault zone in late D_4, when the stress regime was transitional from compressional (D_4) to tensional (D_5). This stress switch is interpreted to be a continuous process, as D_4-deformation and D_5-deformation were caused by the subduction (Zhou et al., 2006) and slab rollback (Zhou and Li, 2000; Zhou et al., 2006; Zhang et al., 2012) of the Paleo-Pacific plate beneath the South China Block. In this process, the approximately E-W-trending σ_1 ($\sigma_1 > \sigma_2 > \sigma_3$) reduced progressively as a response to the rollback of the Paleo-Pacific plate. At the same time, σ_2 also gradually decreased as a result of the simultaneous crust thinning (Jia and Hu, 2002; Jia et al., 2002a, b; Xu et al., 2006). This change of stress eventually led to a stress field with $\sigma_1 > \sigma_2 \approx \sigma_3$ (Fig. 10E), which is supported by the orientations of the ore veins (Figs. 5N and 8N). At this time, the effective stress normal to the Changping fault zone was reduced to the extent that faulting took place, causing seismic activities and breaching the ore fluid reservoir, as depicted by the fault-valve model (Sibson et al., 1988; Sibson and Scott, 1998). While the NE-SW-trending Changping fault zone underwent oblique contraction and dextral strike-slip displacement, as suggested by striations (Fig. 3B), the E-W- to ESE-WNW-trending fracture zones were subject to extension, which created abundant dilation space to drain fluids from the Changping fault zone (Fig. 10E). This process of focused fluid release from depth through the Changping fault zones to the E-W- to ESE-WNW-trending fracture zones may have been repeated multiple times in relation to fluid pressure fluctuated between lithostatic and hydrostatic values, as recorded by the crack-seal texture of auriferous veins (Figs. 6P and 9R).

Finally, a question that remains to be answered is why gold deposits are preferentially hosted in the Precambrian rocks. In addition to the favorable structural conditions to drain the ore fluids as discussed above, the relatively reducing environment in the Precambrian rocks may have played the role of chemical traps. As the ore fluids flowed into the E-W- to ESE-WNW-trending fracture zones, reducing fluids in the country rocks were also sucked toward these structural sites. As the solubility of Fe is relatively high in reducing fluids, the mixing of ore fluids with the Fe-rich reducing fluids may lead to sudden precipitation of large amounts of pyrite and arsenopyrite, resulting in sulfidation, as recorded in the ore veins and wall-rock alteration (Deng et al., 2020). Sulfidation has been suggested as the major mechanism of gold precipitation in the Wangu and Huangjindong gold deposits (Deng et al., 2020).

The above discussions demonstrate that the timing of the initial formation of structures, their orientations and geometries and spatial relationships with each other, and the evolution of regional stress fields, are all important factors that control whether or not and how the structures may be reactivated in the tectonic history of a region, especially in terranes that have been subject to multiple tectonic events. Whether or not a reactivated structure may be mineralized further depends on several factors, the most important being connection with structures linked to the source of the ore-forming fluids and structural-chemical traps that can attract (drain) ore fluids and precipitate ores. In the case of northeastern Hunan, the NE-SW-trending regional Changping fault zone is the critical structure that tapped ore fluids at depth, and the E-W- to ESE-WNW-trending fracture zones developed in the Neoproterozoic meta-sedimentary rocks represent effective structural-chemical traps for gold mineralization. The tectonic conditions favorable for reactivating and connecting these structures were best satisfied in early Cretaceous. Based on this model, E-W- to ESE-WNW-trending fracture zones in the Neoproterozoic meta-sedimentary rocks that are located close to the Changping fault zones, especially those showing evidence of reactivation in early Cretaceous time, would be favorable gold exploration targets. This example demonstrates the importance of understanding the nature of the structural control of mineralization for mineral exploration.

6. Conclusions

1.The gold deposits in northeastern Hunan are hosted by E-W- to ESE-WNW-trending fracture zones developed within meta-sedimentary rocks of the Neoproterozoic Lengjiaxi Group that were first deformed in Neoproterozoic (D_1).

2.The E-W- to ESE-WNW-trending fracture zones were initially formed during the early Paleozoic orogeny (D_2), under a N–S compressional stress regime.

3. The E-W- to ESE-WNW-trending fracture zones were reactivated multiple times in association with different tectonic events, including early Triassic (D_3) and Jurassic to early Cretaceous (D_4).

4.Gold mineralization took place during the reactivation of the E-W- to ESE-WNW-trending fracture zones in the late phase of D_4, when the regional stress field changed from E-W-trending σ_1 ($\sigma_1 > \sigma_2 > \sigma_3$) to E-W-trending σ_1 ($\sigma_1 > \sigma_2 \approx \sigma_3$), in association with the transition of the regional tectonic setting from plate subduction (D_4) to plate roll-back (D_5) of the Paleo-Pacific plate. This stress transition triggered the faulting along the NE-SW-trending regional Changping fault zone, breaching the ore fluids at depth.

5.The E-W- to ESE-WNW-trending fracture zones were favorable for gold mineralization during late D_4 because the extensional reactivation of these fracture zones created structural traps for the drainage of ore fluids episodically released through the Changping fault zone. Furthermore, mixing of the ore fluids with Fe-rich reducing fluids from the Precambrian country rocks facilitated sulfidation and gold precipitation.

6.The gold mineralization in northeastern Hunan provides a good example about how reactivation of pre-existing structures may have played a critical role in gold mineralization in poly-deformation terranes. Understanding the nature of the structural control of mineralization is important for gold exploration.

Declaration of competing interest

The authors declare that they have no known competing financial interests or personal relationships that could have appeared to influence the work reported in this paper.

Acknowledgments

We thank Prof. Stephen Laubach for handling the manuscript and reviewer Prof. Bob Holdsworth, Prof. William Jackson, and an anonymous reviewer for their valuable comments that improved this work. This work was co-funded by the National Natural Science Foundation of China (41930428, 42002090, 41472171), the Hunan Provincial Deep Exploration Research Center of Mineral Resources (DK402-2019-PT01) and the National Key R & D Program of China (2016YFC0600401 and 2017YFC0602302). We thank mine geologists Shenggang Wu, Lei Gao, Wenxiang Wang, Xiaogang Chen, Jinlong Guo, Junhui Chen, Ziwen Ning from Hunan Huangjindong Mining Co. Ltd., Jianbo Wang from Jiangdong Gold Mine, Pingjiang Gold Development Co. Ltd. and Xiuliang Qiu from Kaixin Mining Co. Ltd. for their help in underground tunnel work; senior engineers Zhilin Wen, Jun Wu, and Zhuolong Gao, and junior engineers Lei Ren, Peng Fan and Xiang Wang from Team 402, Hunan

Geology and Mineral Resources Exploration and Development Bureau for assistance in the field work. A particular thank is given to Associate Prof. Jianhua Li and Dr. Chicheng He from Institute of Geomechanics, Chinese Academy of Geological Sciences for their help with stress field reconstruction.

Appendix A. Supplementary data

Supplementary data to this article can be found online at https://doi.org/10.1016/j.jsg.2021.104306.

References

Allmendinger, R.W., Cardozo, N., Fisher, D., 2012. Structural Geology Algorithms: Vectors and Tensors in Structural Geology. Cambridge University Press.

Angelier, J., 1984. Tectonic analysis of fault slip data sets. J. Geophys. Res. 89 (B7), 5835–5848.

Angelier, J., 1994. Fault Slip Analysis and Paleostress Reconstruction. Pergamon Press, Hancock.

Bai, D., Jia, B., Zhong, X., Jia, P., Liu, Y., 2012. Potential genesis of the trending changes of Jinning period and Caledonian structural lineamens in middle-southern Hunan. J. Geomechanics 18, 165–177 (in Chinese with English abstract).

Bai, D., Zhong, X., Jia, P., Xiong, X., Huang, W., Jiang, W., 2015. Progresses in the deformations and tectonic evolutions of the Xuefeng Orogenic Belt and its adjacent areas. Geology and Mineral Resources of South China 31, 321–343 (in Chinese with English abstract).

Carrier, A., Jebrak, M., Angelier, J., Holyland, P., 2000. The silidor deposit, rouyn-noranda district, Abitibi belt:geology, structural evolution, and paleostress modeling of an Au QuartzVein-type deposit in an archean trondhjemite. Econ. Geol. 95, 1049–1065.

Cawood, P.A., Zhao, G., Yao, J., Wang, W., Xu, Y., Wang, Y., 2017. Reconstructing south China in phanerozoic and precambrian supercontinents. Earth Sci. Rev. 186, 173–194.

Charvet, J., Shu, L., Shi, Y., Guo, L., Faure, M., 1996. The building of south China: collision of Yangzi and Cathaysia blocks, problems and tentative answers. J. Asian Earth Sci. 13, 223–235.

Charvet, J., Shu, L., Faure, M., Choulet, F., Bo, W., Lu, H., Breton, N.L., 2010. Structural development of the lower paleozoic belt of south China: genesis of an intracontinental orogen. J. Asian Earth Sci. 39, 309–330.

Chen, X., Rong, J., 1999. From biostratigraphy to tectonics-with ordovician and silurian of south China as an example. Geoscience 201.

Cox, S.F., Wall, V.J., Etheridge, M.A., Potter, T.F., 1991. Deformational and metamorphic processes in the formation of mesothermal vein-hosted gold deposits—examples from the Lachlan Fold Belt in central Victoria, Australia. Ore Geol. Rev. 6 (5), 391–423.

Deng, T., Xu, D., Chi, G., Wang, Z., Chen, G., Zhou, Y., Li, Z., Ye, T., Yu, D., 2020. Caledonian (early paleozoic) veins overprinted by yanshanian (late mesozoic) gold mineralization in the jiangnan orogen: a case study on gold deposits in northeastern hunan, south China. Ore Geol. Rev. 124, 103586 https://doi.org/10.1016/j.oregeorev.2020.103586.

Deng, T., Xu, D., Chi, G., Wang, Z., Jiao, Q., Ning, J., Dong, G., Zou, F., 2017. Geology, geochronology, geochemistry and ore genesis of the Wangu gold deposit in northeastern Hunan Province, Jiangnan Orogen, South China. Ore Geol. Rev. 88, 619–637.

Dichiarante, A.M., Holdsworth, R.E., Dempsey, E., McCaffrey, K.J.W., Utley, T.A.G., 2020. The outcrop-scale manifestations of reactivation during multiple superimposed rifting and basin inversion events: the Devonian Orcadian Basin, N Scotland. J. Geol. Soc. 178, jgs2020-089 https://doi.org/10.1144/jgs2020-089.

Dong, X.F., 2014. Determination and significance of Huangshan orogenic gold deposits in Zhejiang Province. J. Geol. 38 (3), 347–351 (in Chinese with English abstract).

Dong, G., Xu, D., Wang, L., Chen, G., He, Z., Fu, G., Wu, J., Wang, Z., 2008. Determination of mineralization ages on gold deposits in the eastern Hunan province, South China and isotopic tracking on ore forming fluids-redisscussion gold ore deposit type. Geotect. Metallogenia 482–491 (in Chinese with English abstract).

Faure, M., Lepvrier, C., Nguyen, V.V., Vu, T.V., Lin, W., Chen, Z., 2014. The South China block-Indochina collision: where, when, and how? J. Asian Earth Sci. 79, 260–274.

Faure, M., Shu, L., Wang, B., Charvet, J., Choulet, F., Monie, P., 2010. Intracontinental subduction: a possible mechanism for the early palaeozoic orogen of SE China. Terra. Nova 21, 360–368.

Fu, Z., Li, Z., Zheng, D., 1999. Structural pattern and tectonic evolution of NNE-trending strike-slip orogenic belt in the border region of hunan and jiangxi province. Earth Sci. Front. 6, 263–273 (in Chinese with Eglish abstract).

Goldfarb, R.J., Baker, T., Dubé, B., Groves, D.I., Hart, C.J., Gosselin, P., 2005. Distribution, character and genesis of gold deposits in metamorphic terranes. Econ. Geol. Economic Geology 100th Anniversary ume, 407–450.

Goldfarb, R.J., Groves, D.I., 2015. Orogenic gold: common or evolving fluid and metal sources through time. Lithos 233, 2–26.

Han, F., Chang, L., Cai, M., Liu, S., Sun, S., Chen, Y., Peng, Z., Xu, M., 2010. Ore-forming epoch of gold deposits in northeastern Hunan. Miner. Deposits 563–571 (in Chinese with English abstract).

Hao, Y., Li, S., Jin, C., Dai, L., Liu, B., Liu, L., Liu, X., 2010. Caledonian structural characteristics and mechanism in Hunan-Jiangxi-Guangxi provinces. Geotect. Metallogenia 34, 166–180 (in Chinese with English abstract).

He, Y., 1996. Tectono-magmatic activation and gold mineralization in Qinling, China. Geotect. Metallogenia 61–66 (in Chinese with English abstract).

Holdsworth, R.E., Butler, C.A., Roberts, A.M., 1997. The recognition of reactivation during continental deformation. J. Geol. Soc. 154, 73–78.

Holdsworth, R.E., Stewart, M., Imber, J., Strachan, R.A., 2001. The structure and rheological evolution of reactivated continental fault zones: a review and case study. Geological Society, London, Special Publications 184, 115–137.

Hu, R., Cheng, J., Guo, S., Hao, X., 1995. Application of fission track technique to study of gold deposits. Geochimica 24, 188–192 (in Chinese with English abstract).

Huang, C., Fan, G.M., Jiang, G.L., Luo, L., Xu, Z.L., 2012. Structural ore-controlling characteristics and electron spin resonance dating of the Yanlinsi gold deposit in northeastern Hunan Province. Geotect. Metallogenia 36 (1), 76–84 (in Chinese with English abstract).

Ji, W., Faure, M., Wei, L., Yan, C., Yang, C., Xue, Z., 2018. Multiple emplacement and exhumation history of the late mesozoic dayunshan–mufushan batholith in southeast China and its tectonic significance: 1. Structural analysis and geochronological constraints. J. Geophys. Res.: Solid Earth 123, 689–710.

Jia, D., Hu, R., 2002. Lithogeochemical characteristics of mesozoic mafic dikes in northeast Hunan Province. Geotect. Metallogenia 26, 179–184 (in Chinese with English abstract).

Jia, D., Hu, R., Lu, Y., Xie, G., 2002a. Petrological and geochemical characteristics of sodium-rich lamprophyres from Jiaoxiling in northeast Hunan province. Acta Petrol. Sin. 18, 459–467 (in Chinese with English abstract).

Jia, D., Hu, R., Xie, G., 2002b. Petrological geochemistry of the Mesozoic mafic dikes and their implication on tectonic setting in Northeast Hunan Province. J. Mineral. Petrol. 22, 37–41 (in Chinese with English abstract).

Jiao, Q., Deng, T., Wang, L., Xu, D., Chi, G., Chen, G., Liu, M., Chen, Y., Gao, Y., Zou, S., 2017. Geochronological and mineralogical constraints on mineralization of the hetai goldfield in guangdong province, south China. Ore Geol. Rev. 88 https://doi.org/10.1016/j.oregeorev.2017.03.002.

Kerrich, R., Cassidy, K.F., 1994. Temporal relationships of lode gold mineralization to accretion, magmatism, metamorphism and deformation — archean to present: a review. Ore Geol. Rev. 9, 263–310.

Lander, R.H., Laubach, S.E., 2015. Insights into rates of fracture growth and sealing from a model for quartz cementation in fractured sandstones. Geol. Soc. Am. Bull. 127 (3–4), 516–538. https://doi.org/10.1130/B31092.1.

Lawley, C., Imber, J., Selby, D., 2013. Structural controls on orogenic Au mineralization during transpression: Lupa goldfield, southwestern Tanzania. Econ. Geol. 108, 1615–1640.

Lebrun, E., Miller, J., Thebaud, N., Ulrich, S., Mccuaig, C., 2017. Structural controls on an orogenic gold system: the world-class Siguiri gold district, Siguiri Basin, Guinea, West Africa. Econ. Geol. 112.

Li, F.Y., 1990. Metallogenic model and prospecting direction of gold deposit zone in Huangshan. Metal. Geol. 1, 14–18 (in Chinese).

Li, J., Chen, B., An, J., Tan, S., Zhang, X., Yao, Y., 2011. Characteristics of fluid inclusions of the Huangjindong gold deposit, hunan province. Geol. Miner. Resour. South China 27, 163–168 (in Chinese with English abstract).

Li, J., Dong, S., Zhang, Y., Zhao, G., Johnston, S.T., Cui, J., Xin, Y., 2016a. New insights into Phanerozoic tectonics of south China: Part 1, polyphase deformation in the Jiuling and Lianyunshan domains of the central Jiangnan Orogen. J. Geophys. Res.: Solid Earth 121, 3048–3080.

Li, J., Shi, W., Zhang, Y., Dong, S., Ma, Z., 2016b. Thermal evolution of the Hengshan extensional dome in central South China and its tectonic implications: new insights into low-angle detachment formation. Gondwana Res. 35, 425–441.

Li, J., Zhang, Y., Dong, S., Johnston, S.T., 2014. Cretaceous tectonic evolution of South China: a preliminary synthesis. Earth Sci. Rev. 134, 98–136 (in Chinese with English abstract).

Li, J., Zhang, Y., Dong, S., Li, H., 2012. Late mesozoic–early cenozoic deformation history of the yuanma basin, Central South China. Tectonophysics 570–571, 163–183.

Li, P., 2006. Magmatism of Phanerozoic Granitoids in Southeastern Hunan Province, China and its Evolution Regularity. Ph.D. Thesis, Guangzhou Institute of Geochemistry, Chinese Academy of Sciences.

Li, Z., Wartho, J.A., Occhipinti, S., Zhang, C., Li, X., Wang, J., Bao, C., 2007. Early history of the eastern Sibao Orogen (South China) during the assembly of Rodinia: new mica 40 Ar/39 Ar dating and SHRIMP U–Pb detrital zircon provenance constraints. Precambrian Res. 159, 79–94.

Li, Z.H., Chi, G.X., Deng, T., Xu, D.R., 2019. Controls of reactivated faults on the unconformity-related uranium deposits in the athabasca basin, Canada. Geotect. Metallogenia 43, 518–527 (in Chinese with English abstract).

Li, Z.X., Li, X.H., Zhou, H., Kinny, P.D., 2002. Grenvillian continental collision in south China: new SHRIMP U-Pb zircon results and implications for the configuration of Rodinia. Geology 30, 163–166.

Liu, Y., Sun, C., Cui, W., Ji, J., 1989. Study on the occurrence of gold in arsenopyrite of Huangjindong gold deposit in Hunan Province. Contrib. Geol. Miner. Resour. Res. 4, 42–49 (in Chinese with English abstract).

Lu, H.Z., Wang, Z.G., Chen, W.Y., Wu, X.Y., Zhu, X.Q., Hu, R.Z., 2006. Turbidite hosted gold deposits in southeast Guizhou: their structural control, mineralization characteristics, and some genetic constrains. Miner. Deposits 25 (4), 369–387 (in Chinese with English abstract).

Luo, Q.Z., Chen, D.K., 1995. Metallogenic regularity and prospecting progression of gold deposit in north Guangxi. Gold Geol. 1 (2), 14–20 (in Chinese with English abstract).

Luo, X.Q., 1996. Mineralization and prospecting guide of Chanziping gold deposit in Hunan. Hunan Geol. 15 (1), 33–38 (in Chinese with English abstract).

Mao, J., Li, H., 1997. Research on genesis of the gold deposits in the Jiangnan terrain. Geochimica 26 (5), 71–81 (in Chinese with English abstract).
Mao, J., Li, Y., Li, H., Wang, D., Song, H., 1997. Helium isotopic evidence on metalgenisis of mantle fluids in the Wangu gold deposit, Hunan Province. Geol. Rev. 43, 646–649 (in Chinese with English abstract).
Mao, J., Kerrich, R., Li, H., Li, Y., 2002. High 3He/4He ratios in the Wangu gold deposit, Hunan province, China: implications for mantle fluids along the Tanlu deep fault zone. Geochem. J. Jpn. 36, 197–208.
Marrett, R.A., Allmendinger, R.W., 1990. Kinematic analysis of fault-slip data. J. Struct. Geol. 12, 973–986.
Miller, J.M., Wilson, C.J., 2004. Structural analysis of faults related to a heterogeneous stress history: reconstruction of a dismembered gold deposit, Stawell, western Lachlan Fold Belt, Australia. J. Struct. Geol. 26, 1231–1256.
Ortega, O.J., Marrett, R.A., Laubach, S.E., 2006. A scale-independent approach to fracture intensity and average spacing measurement. AAPG (Am. Assoc. Pet. Geol.) Bull. 90, 193–208.
Peng, J., Hu, R., Zhao, J., Fu, Y., Lin, Y., 2003. Sm–Nd dating on scheelites and Ar–Ar dating quartz from Woxi W–Sb–Au ore deposits in western Hunan. Chin. Sci. Bull. 48, 1976–1981 (in Chinese with English abstract).
Qiu, Y., 1999. Tectonic Characteristics and Evolution of the Xufengshan: an Evolution Model for Introcontinental Orogeny. Geological Publishing House, Beijing (in Chinese).
Qiu, Y., Zhang, Y., Ma, W., 1998. Tectonic characteristics and evolution of the Xuefengshan introcontinental orogeny. Geological Journal of China University, pp. 432–433 (in Chinese with English abstract).
Shu, L., Faure, M., Wang, B., Zhou, X., Song, B., 2008. Late palaeozoic–early mesozoic geological features of south China: response to the Indosinian collision events in southeast asia. C. R. Geosci. 340, 151–165.
Shu, L., Wang, B., Cawood, P.A., Santosh, M., Xu, Z., 2015. Early paleozoic and early mesozoic intraplate tectonic and magmatic events in the Cathaysia block, south China. Tectonics 34, 1600–1621.
Shu, L.S., Shi, Y.S., Guo, L.Z., 1995. Plate-Terrane Tectonics and Collisional Orogeny. Nanjing University Press, Nanjing, pp. 94–120 (in Chinese).
Sibson, R.H., 1985. A note on fault reactivation. J. Struct. Geol. 7 (6), 751–754.
Sibson, R.H., 2001. Seismogenic framework for hydrothermal transport and ore deposition. Rev. Econ. Geol. 14, 25–50.
Sibson, R.H., Robert, F., Poulsen, K.H., 1988. High-angle reverse faults, fluid-pressure cycling, and mesothermal gold-quartz deposits. Geology 16, 551–555.
Sun, T., Zhou, X., Chen, P., Li, H., Zhou, H., Wang, Z., Shen, W., 2005. Strongly peraluminous granites of mesozoic in eastern nanling range, southern China: petrogenesis and implications for tectonics. Science in China 48, 165–174.
Wang, C., Shao, Y., Evans, N., Li, H., Zhou, H., Huang, K., Liu, Z., Chen, Y., Lai, C., Liu, Q., 2019. Genesis of zixi gold deposit in xuefengshan, jiangnan orogen (south China): age, geology and isotopic constraints. Ore Geol. Rev. 117, 103301 https://doi.org/10.1016/j.oregeorev.2019.103301.
Wang, J., 2010. Characteristics of Compounding-Combine Fold Superposition and Dynamics of the Xuefengshan Tectonic System. Ocean University of China.
Wang, J., Li, Z., 2003. History of Neoproterozoic rift basins in South China: implications for Rodinia break-up. Precambrian Res. 122, 141–158.
Wang, L., Ma, C., Zhang, C., Zhang, J., Marks, M.A.W., 2014. Genesis of leucogranite by prolonged fractional crystallization: a case study of the Mufushan complex, South China. Lithos 206–207, 147–163.
Wang, Y., Zhang, Y., Fan, W., Peng, T., 2005. Structural signatures and 40Ar/39Ar geochronology of the Indosinian xuefengshan tectonic belt, south China block. J. Struct. Geol. 27, 985–998.
Wen, Z., Deng, T., Dong, G., Zou, F., Xu, D., Wang, Z., Lin, G., Chen, G., 2016. Study on the characters and rules of the ore-controlling structures of the Wangu gold deposit in northeastern Hunan Province. Geotect. Metallogenia 40, 1–14 (in Chinese with English abstract).
Williams, P.F., 1985. Multiply deformed terrains—problems of correlation. J. Struct. Geol. 7, 269–280.
Wu, R., Zheng, Y., Wu, Y., Zhao, Z., Zhang, S., Liu, X., Wu, F., 2006. Reworking of juvenile crust: element and isotope evidence from Neoproterozoic granodioritic in South China. Precambrian Res. 146, 179–212.
Xiao, Y., Chen, G., 2004. Preliminary study on the tectono-metallogenic orientation mechanism of the Dadong-Wangu gold deposit zone, northeastern Hunan province. Geotect. Metallogenia 28, 39–45 (in Chinese with English abstract).
Xiao, Y., Chen, G., Fu, G., 2002. Discussion on the tectonometallogenic background of the Dawan gold ore district, northeastern Hunan Province. Geotect. Metallogenia 26, 143–147 (in Chinese with English abstract).
Xu, D., Chen, G., Xia, B., Li, P., He, Z., 2006. The caledonian adakite-like granodiorites in banshapu area, eastern hunan province, south China: petrogenesis and geological significance. Geol. J. China Univ. 12, 507–521 (in Chinese with English abstract).
Xu, D., Chi, G., Zhang, Y., Zhang, Z., Sun, W., 2017a. Yanshanian (Late Mesozoic) ore deposits in China – an introduction to the special issue. Ore Geol. Rev. 88. S0169136817303293.
Xu, D., Deng, T., Chi, G., Wang, Z., Zou, F., Zhang, J., Zou, S., 2017b. Gold mineralization in the Jiangnan Orogenic Belt of South China: geological, geochemical and geochronological characteristics, ore deposit-type and geodynamic setting. Ore Geol. Rev. 88, 565–618.
Xu, D., Zou, F., Ning, J., Deng, T., Wang, Z., Chen, G., Zhang, J., Dong, G., 2017c. Discussion on geological and structural characteristics and associated metallogeny in northeastern Hunan province, South China. Acta Petrol. Sin. 33 (3), 695–715 (in Chinese with English abstract).
Xu, X., Zhang, Y., Jia, D., Shu, L., Wang, R., 2009. Early mesozoic geotectonic processes in South China. Chinese Geology 36, 573–593 (in Chinese with English abstract).
Ye, M., Li, X., Li, W., Liu, Y., Li, Z., 2007. SHRIMP zircon U–Pb geochronological and whole-rock geochemical evidence for an early Neoproterozoic Sibaoan magmatic arc along the southeastern margin of the Yangtze Block. Gondwana Res. 12, 144–156.
Zhang, Y., Dong, S., Li, J., Cui, J., Shi, W., Su, J., Li, Y., 2012. The new progress in the study of Mesozoic tectonic of South China. Acta Geosci. Sin. 33, 257–279 (in Chinese with English abstract).
Zhang, L., Yang, L., Groves, D.I., Sun, S., Liu, Y., Wang, J., Li, R., Wu, S., Gao, L., Guo, J., Chen, X., Chen, J., 2019a. An overview of timing and structural geometry of gold, gold-antimony and antimony mineralization in the Jiangnan Orogen, southern China. Ore Geol. Rev. 115, 103173 https://doi.org/10.1016/j.oregeorev.2019.103173.
Zhang, Z., Xie, G., Mao, J., Liu, W., Olin, P., Li, W., 2019b. Sm-Nd dating and In-situ LA-ICP-MS trace element analyses of scheelite from the Longshan Sb-Au deposit, Xiangzhong Metallogenic Province. South China. Minerals 9. https://doi.org/10.3390/min9020087.
Zhang, Y., Xu, X., Jia, D., Shu, L., 2009. Deformation record of the change from Indosinian collision related tectonic system to Yanshanian subduction-related tectonic system in South China during the Early Mesozoic. Geoscience Frontiers 234–247 (in Chinese with English abstract).
Zhou, D.Z., Ye, D.Y., Yu, D.L., 1989. A preliminary discussion on the genesis of the Mobin quartz vein-type gold deposit in Hunan Province. Miner. Deposits 8 (1), 51–64 (in Chinese with English abstract).
Zhou, X., Shen, W., Shu, L., Niu, Y., 2006. Petrogenesis of Mesozoic granitoids and volcanic rocks in South China: a response to tectonic evolution. Episodes 29, 26–33.
Zhou, X.M., Li, W.X., 2000. Origin of Late Mesozoic igneous rocks in Southeastern China: implications for lithosphere subduction and underplating of mafic magmas. Tectonophysics 326, 269–287.
Zhou, Y., Dong, G., Xu, D., Deng, T., Wu, J., Wang, X., Gao, L., Chen, X., 2020. The scheelite Sm-Nd age of the Huangjindong Au deposit in Hunan and its geological significance. Geochimica, H202002004 (in Chinese with English abstract).